



Published in final edited form as:

Assay Drug Dev Technol. 2009 October ; 7(5): 440–460. doi:10.1089/adt.2009.0196.

Quantification of lipid droplets and associated proteins in cellular models of obesity via high content/high throughput microscopy and automated image analysis

Patrick M. McDonough^{1,#}, Ramses M. Agustin², Randall S. Ingermanson¹, Patricia A. Loy¹, Benjamin M. Buehrer³, James B. Nicoll³, Natalie L. Prigozhina², Ivana Mikic², and Jeffrey H. Price

¹Vala Sciences Inc, San Diego, CA 92121, 858 200 9520, 858 581 6275, fax 858 581 6277

²The Burnham Institute for Medical Research, La Jolla, CA 92037, Ph 858 646 3100, fax 858 646 3199

³Zen-Bio, Inc, Research Triangle Park, NC 27709, 866-234-7673, fax 919-547-0693

Abstract

Intracellular lipid droplets are associated with a myriad of afflictions including obesity, fatty liver disease, coronary artery disease and infectious diseases (e.g., HCV and tuberculosis). To develop high content assay (HCA) techniques to analyze lipid droplets and associated proteins, primary human pre-adipocytes, were plated in 96-well dishes in the presence of rosiglitazone (rosi), a PPAR γ agonist which promotes adipogenesis. The cells were then labeled for nuclei, lipid droplets, and proteins such as perilipin, protein kinase C (PKC), and hormone sensitive lipase (HSL). The cells were imaged via automated digital microscopy and algorithms were developed to quantify lipid droplet (Lipid Droplet algorithm) and protein expression and colocalization (Colocalization algorithm). The algorithms, which were incorporated into Vala Science Inc's CyteSeer[®] image cytometry program, quantified the rosi-induced increases in lipid droplet number, size, and intensity, and the expression of perilipin with exceptional consistency (Z' values of 0.54 to 0.71). Regarding colocalization with lipid droplets, Pearson's Correlation coefficients of 0.38 (highly colocalized), 0.16 (moderate), and -0.0010 (random) were found for perilipin, PKC, and HSL, respectively. For hepatocytes (AML12, Huh7, and primary cells), the algorithms also quantified the stimulatory and inhibitory effect of oleic acid and triacsin c on lipid droplets (Z's > 0.50) and ADFP expression/colocalization. Oleic-acid induced lipid droplets in HeLa cells and macrophages (THP-1) were also well quantified. The results suggest that HCA techniques can be utilized to quantify lipid droplets and associated proteins in many cell models relevant to a variety of diseases.

Introduction

Obesity in modern society has reached "pandemic" proportions and may be as high as 30% in the general US population^{1–4}. Alarming, there is a high incidence of obesity in children and adolescents^{5–7} indicating that obesity will be a significant health problem for the foreseeable future. In addition to reducing mobility, obesity is an underlying factor associated with a variety of life-threatening pathologies including diabetes, heart disease, and liver malfunction.

#Corresponding author Patrick M. McDonough, Vala Sciences Inc, 3030 Bunker Hill St., STE 201, San Diego, CA 92109, 858 581 6275, fax 858 581 6277, pmcdonough@valasciences.com.

The cellular basis of obesity is increased triglyceride accumulation within adipocyte lipid droplets. Also, increased accumulation of lipid droplets within hepatocytes (steatosis) is the defining characteristic of both alcoholic- and non-alcoholic fatty liver disease (NAFLD), conditions that can progress to cirrhosis and liver failure^{8, 9}. Ominously, 20 to 35% of the general adult population in the US may have NAFLD, and the incidence in obese individuals is approximately 75%¹⁰. NAFLD is closely associated with diabetes and the Metabolic Syndrome^{8, 11, 12}. Steatosis is also present in 50% of the patients infected with HCV¹³ and association of viral proteins with lipid droplets may be critical for viral replication¹⁴. Lipid droplets are also prominent features of skeletal muscle cells¹⁵, cardiac myocytes^{16–18}, and pancreatic β -cells^{19, 20}. Lipid droplets within macrophages also play a critically important role in the etiology of coronary artery disease, as the accumulation of cholesterol esters within lipid droplets is a defining cellular event leading to production of “foam” cells and atherosclerotic plaques^{21, 22}. Lipid droplets (lipid bodies) within macrophages are also implicated in the etiology of tuberculosis^{23, 24}. Thus, in general, cells expressing an abnormally large number of lipid droplets are often impaired in function and associated with disease pathologies. An interesting exception is skeletal muscle, in which endurance exercise increases lipid droplet content²⁵. An emerging hypothesis is that lipid overload leads to “lipotoxicity” and this may underlie the broad manifestations of the Metabolic Syndrome^{26–28}. Development of novel tools to investigate lipid droplet and fatty acid metabolism are thus likely to be of interest to researchers in a variety of biomedical contexts.

Nascent lipid droplets form by the accumulation of neutral lipid within the membrane bilayer of the endoplasmic reticulum^{29–31}. In early stages of adipogenesis, lipid droplets nucleate at many loci throughout the cell, and, as the adipocytes mature, the lipid droplets coalesce, typically into one large centrally located droplet³². Every step of lipid droplet formation and metabolism is regulated or influenced by proteins that associate with the lipid droplets. PAT proteins (named after the founding members of the family, which are perilipin, adipose differentiation-related protein (ADFP/adipophilin/perilipin2), and TIP47) are commonly associated with lipid droplets and orchestrate their formation and maturation^{29–31, 33, 34}. PAT proteins are expressed in a tissue-specific manner, with perilipin expression restricted to adipocytes and steroidogenic cells. ADFP is also expressed in liver, and is upregulated in fatty liver disease^{34–36}.

Fatty acids are released from lipid droplets via the action of lipases which include hormone sensitive lipase (HSL) and the adipocyte triglyceride lipase (ATGL) family members^{37–40}. Perilipin may form a functional barrier to lipolysis, as lipolysis is increased in mice in which perilipin has been knocked out⁴¹. Furthermore, perilipin is phosphorylated by cAMP-dependent protein kinase (PKA)⁴², and this is associated with translocation of perilipin from the lipid droplets to the cytoplasm in certain adipocyte model systems^{43–45}. Elevated cAMP, resulting from beta-adrenergic stimulation, also leads to translocation of HSL from the cytoplasm to the lipid droplets in adipocytes^{44, 46}. Perilipin may also help regulate lipolysis by ATGL⁴⁷. Thus, regulation of lipolysis is often associated with translocation of perilipin and lipases between the lipid droplet and cytoplasm.

The lipid droplet proteins discussed above likely represent just the “tip of the iceberg” regarding the proteins that associate with droplets and modulate triglyceride metabolism. Proteomic techniques have been used to enumerate the variety of lipid droplet-associated proteins in yeast⁴⁸, 3T3-L1 cells⁴⁹, and 248 separate lipid-droplet associated proteins have been identified in *Drosophila*⁵⁰. A similar approach has also been applied to mammalian hepatocytes⁵¹. Lipid droplets likely represent “organizing centers” of the metabolic enzymes involved in triglyceride metabolism and are dynamically regulated in response to the energetic demands of the cells and organism. Given their emerging recognition of their importance, lipid droplets and associated proteins will undoubtedly be studied in ever increasing detail for years to come.

High content analysis (HCA) is an emerging technology in which candidate pharmaceuticals or genomic (RNAi or cDNA) libraries are tested for potential beneficial effects via assays performed on cells cultured on microtiter plates^{52–65}. The cells are then stained or labeled to visualize structures or proteins and photographed via robotic digital microscopy workstations. The images are analyzed for information by algorithms designed to identify and extract information relevant to cell/disease model^{66–69}. Advances in automatic acquisition, measurement, comparison and pattern classification tools for cellular images continue^{69–77}. The concept that digital images from both conventional and confocal microscopy can be analyzed by an evolving set of sophisticated image-analysis algorithms is advancing, not only in the context of chemical and siRNA screening, but, also in the context of modern quantitative approaches to microscopy-based cellular phenotypic characterization^{78, 79}. Thousands of images representing hundreds of thousands of individual cells can be acquired via HCA workstations in a single experimental session. For example, a chemical library representing 109,000 compounds was recently screened for their ability to inhibitors of phagocytosis ([PubChem BioAssay 1029](#)). Of key importance are continued advances in quantitative image analysis algorithms that can extract the potential wealth of information contained within cell-based images relevant to understanding the disease state and identifying effective therapeutic compounds.

Lipid droplet metabolism represents an ideal subject for HCA, since, as discussed above, lipid droplets pervade an exceptional number of human pathologies. Furthermore, information relevant to disease states includes not only the number and size of the lipid droplets, but also the expression level and cellular location of proteins that associate with the lipid droplets. With the overall goal of developing HCA cytometry algorithms relevant to lipid droplet metabolism, the present study was conducted utilizing cell types which included primary human adipocytes, cells derived from hepatocytes (AML12 and Huh-7 cells), primary hepatocytes, HeLa, and a differentiated macrophages (THP-1 cells). For the adipocytes, the phenomenon of PPAR γ - induced adipogenesis was examined. For the hepatocytes, HeLa, and macrophages, lipid droplets were induced by addition of fatty acids to the culture media. The results demonstrate that quantitative image analysis techniques can be used to quantify lipid droplets and lipid-droplet associated proteins in a variety of cell contexts with great importance to human health.

Methods

Cell culture

Human preadipocytes were supplied from liposuction procedures by Zen-Bio (Research Triangle Park, NC). AML12, Hep G2, HeLa, and THP-1 cells were obtained from ATCC. Huh-7 cells were obtained from the Japan Health Sciences Foundation, Health Science Research Resources Bank. Primary rat hepatocytes were a generous gift of RegeneMed (San Diego, CA). Human preadipocytes were plated (13,000 cells/well, passage 2) on glass-bottomed 96-well dishes (Nunc) precoated with gelatin that was cross-linked with glutaraldehyde. To coat the dishes, wells were incubated with 1% porcine gelatin (Sigma G1890) for 15 minutes. Excess fluid was then aspirated, and 10 μ l of a 0.5% glutaraldehyde solution was added to each well. Wells were then extensively rinsed (3X) with PBS, incubated with DMEM + 10% FBS for 60 minutes, and rinsed 2X with phenol-red free culture medium (Gibco #31053-028). For AML12 (20,000 cells/well, passage 11 to 15), Hep G2, Huh-7 (20,000 cells/well, passage 50), HeLa (20,000/well), and THP-1 cells (20,000/well, passage 2 to 4), the wells were incubated with a 1/50 dilution of Matrigel, for 60 minutes, and rinsed 1X with PBS prior to plating.

Lipid staining and protein labeling

Following exposure to test chemicals, cells were rinsed with PBS, and fixed with 4% paraformaldehyde (15 minutes, room temperature), followed by 15 minutes permeabilization

with either 0.1% Triton-X (adipocytes) or 0.01% saponin (other cell types) plus 0.1% BSA prepared in PBS. Permeabilization and all other steps were performed with rotation at 37° C. After fixation, cells were incubated with Vala Science's Lipid Staining reagent prepared in blocking buffer (10% normal goat serum, 3 % bovine serum albumin, 0.02% sodium azide, in PBS) for 30 minutes to label neutral lipids in the green fluorescence channel. The samples were then rinsed 3 times with PBS, and stained for nuclei by incubating for 20 minutes in DAPI (250 ng/ml DAPI prepared in 10 mM Tris, 10 mM EDTA, 100 mM NaCl, 0.02% sodium azide, buffered to pH 7.4).

Vala Sciences Inc's Perilipin and PKC reagent kits were used to label perilipin and PKC, which were visualized in the red fluorescent channel. For HSL, a chicken polyclonal was used (Chemicon, Ab3525) which was visualized with an Alexa594-goat anti-chicken (Molecular Probes, A11042). A goat polyclonal antibody obtained from Dr. Constantine Londos (NIH) was used to visualize ADFP in combination with a Cy3 donkey anti-goat antibody (Chemicon, AP180C).

Image acquisition

Images were acquired with a Q3DM Eidaq 100 robotic microscopy instrument (equivalent to the Beckman Coulter IC 100) running Beckman Coulter's CytoShop 2.0. This instrument includes a Nikon Eclipse microscope with an automated stage interfaced to a fluorescence light source and filter wheel and cubes with filters for UV (DAPI), FITC, and rhodamine fluorescence. The workstation features a Windows computer, which controls stage positioning, and data acquisition. Images were acquired with a Hamamatsu Orca ERG progressive scan 1344×1024 cooled interline CCD camera, utilizing 2 × 2 binning. Typically, 4 images (representing a 2 × 2 contiguous image set) were acquired in the center of each well with either a 20× 0.5 NA (resulting in 0.6848 × 0.6848 μm²/pixel) or a 40× 0.75 NA "dry" objective (resulting in 0.344 × 0.344 μm²/pixel). Images were stored as gray-scale bit mapped images (*.bmp).

Quantitative triglyceride assay

Triglyceride was measured using a total triglyceride assay kit (Zen-Bio, inc.). Cultured cells were washed with buffer to remove residual medium and the cells lysed with lysis buffer. Accumulated triglyceride was digested with lipase for up to 3 hours to release glycerol into the buffer. Aliquots were then removed and the amount of glycerol measured using Reagent A (Zen Bio, Inc.). The assay determines the amount of glycerol liberated from triglycerides by spectrophotometric detection at 540 nm and is linear over a glycerol concentration range of 0 to 200 μM.

Chemicals, drugs and antibodies

DMEM was obtained from Media Tech Inc., and CellGro, respectively. Matrigel was from BD Biosciences (Cat. # 354234). Triacsin C was from Biomol. (Cat # EI-218). Phorbol-12-myristate-13-acetate, used to induce differentiation of the THP-1 cells was from Cal Biochem (catalogue 524400).

Data nomenclature

The nomenclature in CyteSeer® (Vala Sciences Inc, San Diego, CA) was developed to facilitate data reporting. During image acquisition, the same field of view was typically imaged in 3 separate optical channels, to selectively visualize the nuclei, lipid droplets, and protein; thus, the three images channels were abbreviated as the Ni, Li, and Pi, respectively (Table 1). From the nuclear image, the nuclear analysis algorithm identified the pixels associated with each nucleus, which defined the nuclear mask, Nm. Furthermore, from the size, position, and

shape of the nuclei, the boundaries of each cell were estimated, to yield the whole cell mask, W_m . The cytoplasmic mask, C_m , was defined as W_m minus N_m . The lipid droplet mask, L_m , was defined all pixels associated with a cell identified as lipid droplets by the Lipid Droplet algorithm. Similarly, pixels identified as above threshold in the protein image by the Colocalization algorithm were defined as the protein mask, P_m . The areas of each mask were reported on a “per cell” basis, as was the lipid droplet count (LDC). The mean diameter of the droplets (LDD) was estimated using a root mean square procedure.

For a given image and mask, three separate intensity parameters were reported, which included the total integrated pixel intensity (T_{ii}), the average pixel intensity (A_{pi}) and the median pixel intensity (M_{pi}). Colocalization data was also reported between the lipid and protein images, corresponding to the Pearson’s Correlation (P_r), and the Manders’ colocalization coefficients M_1 and M_2 ⁸⁰. Additional colocalization coefficients, corresponding to the Manders’ Overlap and Split Overlap coefficients were also encoded in the Colocalization Algorithm, but were not used in the present report. To represent the data parameters, the pixel intensity (or colocalization coefficient) is listed first followed by the image then mask. Thus, $T_{ii} Li Lm$ is the total integrated pixel intensity for the lipid image and lipid mask, and “ $P_r Li Pi Wm$ ”, is the Pearson’s correlation, lipid image, protein image, whole cell mask. In all, 62 different data parameters were reported for each cell by CyteSeer®’s Lipid Droplet algorithm; the Colocalization Algorithm reported an additional 15 parameters relating to the protein channel and colocalization between the lipid and protein. Reports were created as *.csv files which were uploaded into Excel for analysis and included cell by cell readouts, in which data parameters were reported for every cell in a well, and well by well readouts, which represented the data averaged across all cells imaged in a well (see Table 2).

Statistical analysis

To quantitatively assess the suitability of the various assays for subsequent use in HCA screening applications, Z' values were calculated. Z' is an index of the dynamic range of an assay, which is a function of the ratio of the sum of variabilities of the maximum and minimum control values and the difference between their means⁸¹,

$$Z' = 1 - \frac{3(\sigma_+ + \sigma_-)}{|\mu_+ - \mu_-|},$$

where σ_+ and σ_- are the standard deviations (SDs) of the positive and negative controls, respectively, and μ_+ and μ_- are the corresponding means, respectively. Z' has a theoretic range of negative infinity to 1.0 (an ideal assay in which there is no standard deviation and finite separation between means would yield $Z' = 1.0$). Z' values > 0.2 are considered very good for an assay, and Z' are conceptually much more stringent than a $p < .05$ determination from a t-test (Z' can be negative, yet p could be $< .05$). Assays in which $Z' > 0.50$ are considered excellent for high throughput screening applications involving thousands to hundreds of thousands of test compounds, as there is very little chance that false positive hits will arise from random variation in the data.

Statistical tests used to test for differences between experimental groups included ANOVA, followed by the post hoc tests Dunnett’s test or Newman Keuls, and were performed with GraphPad Prism version 5.02. EC_{50} and IC_{50} determinations were performed using the least-squares curve fitting, log agonist v. responses (three parameter) option of GraphPad.

CyteSeer Algorithms

The Lipid Droplet Algorithm in Vala Science's CyteSeer® Image analysis platform program uses the nuclear and lipid images to quantify the lipid droplets associated with each cell in the field of view. The algorithm was first developed with images obtained from human subcutaneous preadipocytes exposed to different doses of rosiglitazone (rosi), an anti-diabetic PPAR γ agonist which strongly induces lipid droplet formation in this cell type, which were very well visualized by fluorescence microscopy (Figure 1A and B). The prototype algorithm was developed in Matlab (Mathworks). Images were convolved with the 7 \times 7 "Mexican top hat" filter⁸² to enhance contrast, and further intensity thresholded into binary masks of the lipid droplets (Figure 1C and 1D). Matlab functions were used to calculate the area, the number, equivalent circle radius, the average intensity and the standard deviation of the intensity of each lipid droplet. To validate results from the Lipid Droplet algorithm, samples cultured in an identical fashion were assayed for total triglycerides. Rosiglitazone was found to increase triglyceride production (as assayed biochemically) and lipid droplets (as assayed with the Lipid Droplet algorithm) with very similar dose-response relationships (Figures 1E and F). Rosiglitazone also increased lipid droplet size and lipid staining intensity with a similar dose-response relationship (data not shown). Thus, the Lipid Droplet algorithm was ported into JAVA and incorporated into Vala Science's CyteSeer® Image analysis platform program.

Proteins that associate with lipid droplets are of high interest to the biomedical community as they control triglyceride metabolism and related processes. Thus, a related algorithm was developed (the Colocalization algorithm) to quantify the expression level of a protein visualized in a third channel, along with the degree to which the protein colocalizes with the lipid droplets. To generate cell samples for prototyping purposes, human preadipocytes were exposed for 19 days to a proprietary PPAR γ agonist from Zen-Bio to induce lipid droplet formation, then fixed and stained, as above, utilizing the Vala Lipid Staining reagent. The cells were then labeled for perilipin, which was found closely associated with the majority of the lipid droplets in cells treated with the PPAR γ agonist.

CyteSeer® is Vala's successor to Thora™, both of which perform true cell-by-cell cytometry^{70, 83}. CyteSeer® incorporates a user-friendly GUI, cross-platform compatibility (PC, MacIntosh, and Linux operating systems), improved data storage and the Lipid Droplet and Colocalization algorithms⁸⁴. CyteSeer®'s novel image viewer (free via download from Vala's website) displays images in user-selectable colors, as well as controls zoom and contrast. User-controlled sensitivity settings enable adjustment of the images segmentation algorithms to enable "fine-tuning" for differences between brightness, contrast and signal-to-noise levels between various sets of images. An example field of view obtained from human preadipocytes exposed to a proprietary PPAR γ agonist, is shown in Figure 2. The Lipid Droplet algorithm produced a mask that identified the lipid droplets with good fidelity (compare Figures 2A and 2B). Small outlying spots in the lipid mask typically represent small dim droplets in the original images. The perilipin label is very closely identified with the outer edges of the lipid droplets (Figure 2C), and was well identified by the Colocalization algorithm (Figure 2D). The protein mask, determined from the perilipin image, often coincides with entire lipid droplets, rather than just the edges of the droplets, which may be somewhat contrary to expectation. However, for the perilipin images, the pixel intensity values within the center of the lipid droplets are often significantly higher than the overall background of the images, leading to assignment of these pixels to the protein mask. The Lipid droplet algorithm estimates the likely center point of each lipid droplet as the "Seed Mask" (Figure 2E); typically, each droplet identified by visual inspection of the image was also represented by a single point.

To enable cell-by-cell analyses, and to estimate the boundaries between the cells, a variation of Vala's proprietary Membrane algorithm⁸⁴ tessellates cell border estimates and enables measurements of cell position, size, and pseudo-cell-boundaries between the nuclear images.

Since lipid droplets in adipocytes are typically closely associated with the nucleus, the tessellation-based algorithm performs reasonably well at assigning lipid droplets to the correct cell (Figure 2F), as judged by visual inspection. Thus, by using the Lipid Droplet, Colocalization, and the Membrane Tessellation algorithms, CyteSeer® quantifies lipid droplets and perilipin expression on a true cell-by cell basis.

Human preadipocytes, especially those that have just begun the adipogenesis program, often feature small lipid droplets that label much more dimly than the larger lipid droplets typically found in more mature cells. Such lipid droplets are readily identified by CyteSeer® and can be viewed by increasing the “contrast” adjustment of the Image Viewer (Figure 3). The sensitivity of CyteSeer®’s algorithms can be adjusted for optimal quantification of images obtained under different conditions of labeling intensity and magnification.

Results

Quantification of lipid droplets in human adipocytes in an automated fashion by CyteSeer®

To test the hypothesis that CyteSeer® could quantify lipid droplets within adipocytes on a cell by cell basis under conditions appropriate for high throughput screening, human subcutaneous preadipocytes were plated on a 96 well dish and exposed to rosi at concentrations ranging from 0 to 3000 nM for 9 days; the cells were then fixed, permeabilized, and labeled for nuclei and lipid droplets using Vala reagents, and imaged with a Beckman IC100 Image Cytometer. Note that the 9 day exposure period represents a relatively short time period for exposure to rosiglitazone, as 14 to 21 days of exposure are required for full maturation of the adipocyte phenotype. The shorter time point was chosen because the Lipid Droplet algorithm accurately identifies small lipid droplets that arise early during the adipogenesis program (see above). Also, since cells in outer wells of 96-well plates tend to behave inconsistently, perhaps due to differential evaporative or other “edge effects” (unpublished observations), cells in the outer wells were not treated with rosi, and were not considered for analysis.

In the absence of rosi, 26.1% of the preadipocytes developed lipid droplets (Figure 4A). The percentage of cells expressing lipid droplets increased as a function of rosi concentration reached a maximum of 72.9% (approx. 3-fold of control) in the presence of 1000 nM rosi, and the EC50 for this effect was 55.9 nM. Many other data parameters derived from the lipid image also increased in a similar manner, including LDC (which increased from approximately 1/cell to 4/cell), the LDD (which increased from 2 to 9 μm), and Api Li Lm (which increased from 22 to 91 pixel intensity units) (Figure 4B–4D). Ar Pm, the area of the Protein mask (in this case for perilipin), also increased with a similar dose-response and fold stimulation (increased 4-fold by 1000 nM rosi, Figure 4E). For all of these data parameters, Z’ values ≥ 0.54 as calculated between the cells exposed to 0 vs. 1000 nM rosi. These high Z’ values are exceptionally high, especially for cell-based assays, and indicate that the methodology is suitable for high throughput screening. Furthermore, since such high Z’ values can only be achieved when there is relatively little variability between the control and maximally stimulated samples, the assay proved to be exceptionally sensitive to effects of low concentrations of rosi. For example, a statistically significant increase ($p < 0.05$ vs. 0 rosi) in LDC was achieved with rosi = 1 nM (1×10^{-9} M, Figure 4B) and 10 nM rosi led to statistically significant increases in the percentage of cells with lipid droplets (Figure 4A), LDD, and Ar Pm (Figure 4E). Lipid droplets obtained with 3000 nM rosi were reduced compared to the values obtained with 1000 nM rosi, suggesting that there may be a toxic effect associated with the higher concentration.

Colocalization analysis of lipid droplets and proteins

A goal of the project was to develop the methodology to quantify colocalization between lipid droplets and proteins as this is of high interest in the lipid droplet field; additionally, quantifying

subcellular locations of cellular structures or proteins is a potential strength of the HCA approach and very relevant to control of lipid metabolism. To test this approach, preadipocytes exposed to the proprietary PPAR γ agonist for 14 days were visualized for lipid droplets and for proteins that varied in the degree to which they associate with lipid droplets, which included hormone sensitive lipase (HSL), protein kinase C α , or perilipin.

Unlike perilipin, HSL labeling did not colocalize with the droplets under the conditions used in this study; instead, HSL label was distributed throughout the cellular compartments, in a finely granular manner (Figure 5A–5C). Consistent with the nature of the distribution of the HSL label, the P_r values calculated between the lipid and the HSL images were near zero, or slightly negative (see Figure 5 for representative images and Table 3 for data). The results imply that the HSL label is randomly distributed with respect to the lipid stain. It has been established that β -adrenergic stimulation elicits migration of HSL to the lipid droplets in certain adipocyte-model systems⁴⁶, and developing techniques to quantify this translocation is in progress (unpublished results). For the present study, the images representing HSL provide examples in which the labeling pattern is not associated with the lipid droplets, in contrast to the strong lipid-droplet-associated labeling pattern obtained with perilipin.

Interestingly, the images of PKC distribution somewhat resemble the images of HSL, in that PKC is distributed throughout the cell; however, close examination reveals that the brightest labeling for PKC often occurred at the edges of the lipid droplets (Figure 5D–F); P_r Li Pi Wm values of 0.156 to 0.167 were found (Figure 5F and Table 3), suggesting a mild association of PKC with the lipid droplets.

As is widely known and shown above, perilipin is closely associated with lipid droplets and scarcely detectable at other cellular locations; the P_r Li Pi Wm ranged from 0.322 to 0.429 for perilipin for this experiment, which were the highest values obtained for the experiment. This indicates partial colocalization of perilipin with the lipid label. A partial, rather than perfect, colocalization is expected since perilipin is localized on the edges of the droplets, but not within the center of the droplets where the lipid staining is the brightest. Thus, within the context of the entire cell, perilipin is colocalized with the lipid droplets; however, within the context of individual lipid droplets, perilipin expression is brightest near the edges of the droplets, where the lipid stain is faintest. P_r Li Pi Wm for perilipin did not appreciably change with the dose of rosi; thus, perilipin was always associated with lipid droplets, even under conditions in which perilipin and lipid droplet expression was low. This is consistent with the hypothesis that lipid droplets help stabilize perilipin, protecting it from degradation⁸⁵.

Since the P_r Li Pi Wm values in this experiment were consistent for each dose of rosi, the values obtained for each protein obtained at the different concentrations of rosi were averaged, then analyzed for statistically significant differences vs. the other proteins. The average P_r Li Pi Wm values obtained for each protein differed from one another at $p < 0.05$ (Table 3, Exp. #1, final column).

In a related experiment, adipocytes treated with rosi (1000 nM) were stained for lipid droplets and labeled for perilipin or stained for HCS CellMaskTM, a compound that is visualized in all cellular compartments. In this experiment (Table 3, experiment 2), the P_r Li Pi Wm values for perilipin averaged 0.480. In contrast, HCS CellMaskTM, which was distributed throughout the cell, including the nucleus yielded an average P_r Li Pi Wm value of 0.186, and the results for HCS CellMaskTM were significantly different from the perilipin values. Overall, these data demonstrate that P_r can be used to quantify the association of proteins with the lipid droplets, and this can be done in an automated fashion as part of an HCA procedure.

Quantification of lipid droplets in hepatocytes

The image and data analysis strategies discussed above were developed to quantify lipid droplets and associated proteins that appear in adipocytes during the adipogenesis process. Hepatocytes also feature small lipid droplets, and such lipid droplets are the causative factor in fatty liver disease and may participate in the pathological responses elicited by HCV. To test if the Lipid Droplet and Colocalization Algorithms can quantify lipid droplets and associated proteins in hepatocytes, experiments were carried out with AML12 cells, a murine hepatocyte-derived cell line, and also with Huh-7 and HepG2 cells, which are derived from human hepatocytes. A small pilot experiment was also carried out with primary rat hepatocytes. In these experiments the cells were incubated in the absence or presence of oleic acid, and stained for lipid droplets as well as for ADFP, a protein that is prevalent in hepatocytes that is known to associate with lipid droplets.

Control AML12 cells, maintained in the absence of oleic acid, expressed relatively few lipid droplets (Figure 6A) but did feature significant ADFP labeling as an overall diffuse cytoplasmic label that also included numerous punctate structures (Figure 6B); the punctual regions of ADFP label often correlated with lipid droplets, but much of the ADFP label did not obviously coincide with lipid staining. When images from control cells were analyzed and the masks developed for the lipid droplets and ADFP are compared, certain lipid droplets were colabeled (as yellow regions in Figure 6C), but much of the ADFP label was independent of the labeled lipid droplets. For oleic acid-treated AML12 cells, lipid droplets were abundant and distributed throughout the cell (Figure 6D). Also, the ADFP label was brighter than for control cells, and the ADFP label was closely associated with the lipid droplets (Figure 6D and 6E). Masks developed for the lipid droplets and ADFP for oleic acid-treated AML12 showed extensive overlap (Figure 6F). Cells exposed to oleic acid plus a maximally effective concentration of triacsin C (5.4 μM), an inhibitor of acyl-CoA synthetase, exhibited a phenotype much like cells cultured in the absence of oleic acid (Figure 6G– 6J). The inhibitory effect of triacsin C on lipid droplet formation is consistent with the likely role of acyl-CoA synthetase in lipid droplet formation.

As quantified by the Lipid Droplet algorithm for AML12 cells visualized with a 20X objective, control cells featured an average 1.1 lipid droplets per cell and oleic acid elicited an approximate 4-fold increase in the number of lipid droplets (Figure 7A). Oleic acid also elicited a 21.6-fold increase in the area of the lipid droplet mask/cell (Figure 7B), a 21.0-fold increase in the ratio of the area of lipid mask to the whole cell area (Figure 7C), and a 25.7-fold increase in the total integrated intensity of the lipid mask/cell (TLL, Figure 7D), which represented the greatest fold-response among the data parameters. Data from this multi-comparison experiment was analyzed statistically via ANOVA followed by Newman Keuls post hoc analysis, which compares each condition in the experiment to every other condition in a pair-wise manner. For all data parameters, the effect of oleic acid was highly statistically significant ($p < 0.001$) vs. the control cells (no oleic acid). Triacsin C inhibited the effect of oleic acid with an IC_{50} of approximately 1 μM (the IC_{50} values for the data parameters Ar Lm, ArLM/AR Wm and Tii Lii Lm were 1.15 μM , 1.00 μM , and 0.86 μM , respectively), and statistically significant inhibitory effects ($p < 0.05$, compared to oleic acid, alone) of triacsin C vs. oleic acid were found for doses as low as 0.08 μM (for the data parameter ArLm/Ar Wm, Figure 7C).

The data for the AML12 cells was exceptionally consistent. Z' values of 0.74, 0.72, 0.86, and 0.82, were obtained, respectively, for LDC, Ar Lm, Ar Lm/Ar Wm, and Tii Li Lm for the effect of oleic acid for the data depicted in Figure 7. The inhibitory effect of triacsin C on oleic acid-induced lipid droplet formation was also quantified with very low variability, especially for the Tii Li Lm parameter, yielding a Z' value of 0.64 for the effect of triacsin C on Tii Li Lm (Figure 7D). These data demonstrate that AML12 cells will likely be very useful for screens conducted to identify compounds that either stimulate lipid droplet formation, when added

alone, or antagonize oleic acid-induced lipid droplet formation, if added in the presence of oleic acid. Thus, the cell line appears ideal for identifying chemical probes for the lipid droplet formation pathway, and identifying chemicals that may antagonize hepatic lipid droplet formation, which might be relevant to fatty liver disease.

Lipid droplets in the Huh-7 human hepatocyte cell line were also very well visualized (data not shown), and these were quantified with good consistency by CyteSeer®. Huh-7 cells cultured in the absence of oleic acid featured an average of 4 lipid droplets/cell, and lipid droplet count was increased approximately 2-fold by oleic acid (Figure 7E). Thus, Huh7-cells feature a greater number of lipid droplets/cell than AML12 cells under basal conditions. Oleic acid elicited a 3.3-fold increase in Tii Li Lm for Huh-7 cells (Figure 7F). The effect of oleic acid was highly significant on all data parameters ($p < 0.001$). Triacsin C inhibited the effect of oleic acid on LDC and Tii Li Lm with a IC50s of 0.42 μM and 0.33 μM and the inhibitory effect of 0.08 μM triacsin C in the presence of oleic acid was highly significant ($p < 0.001$) for both data parameters. Excellent Z' values were obtained for both the effect of oleic acid (0.66) and the effect of triacsin C in the presence of oleic acid ($Z' = 0.58$, Figure 7F). Thus, Huh-7 cells are also a likely candidate for high throughput screens designed to identify chemical probes for the lipid droplet pathway, or to identify potential inhibitors of hepatic lipid droplet formation.

Colocalization analysis of lipid droplets and ADFP in hepatocytes

To quantify the colocalization of lipid droplets with ADFP, the plate from the previous experiment with AML12 cells was imaged with a 40X objective and the images analyzed by CyteSeer®'s Colocalization algorithm. To simplify the data presentation, the results are shown only for the control cells and for the cells treated with oleic acid, alone (Figure 8). Since additional sample groups were present in the complete data set (e.g., samples representing wells exposed to oleic acid plus lower doses of triacsin C), the data set from images scanned at 40X were statistically analyzed with Dunnett's Multiple Comparison's procedure which can be used to compare the control groups with selected experimental groups in multiple comparison experiments. For the images obtained at 40X, an average of 3.4 lipid droplets/cell were observed for the control cells, and this was increased 4.4 fold by oleic acid (Figure 8A). The greater number of lipid droplets/cell in this experiment vs. the experiment depicted in Figure 7 is likely due to the use of a higher powered objective (40X) for image acquisition in this experiment (a 20X objective was used previously). Lipid droplets tend to occur in clusters in AML12 cells. These clusters can appear as a large single droplet (sometimes irregularly shaped) at low magnification, but are resolved into discrete smaller droplets by higher magnification. Thus, imaging at a higher magnification yields a greater number of droplets per cell. Tii Li Lm was increased 81-fold by oleic acid with a Z' value of 0.64 (Figure 8B). The area of the cell identified as ADFP-positive by the Colocalization algorithm, was increased 2-fold by oleic acid (Figure 8C). The effects of oleic acid on LDC, Tii Li Lm, and Ar Pm were significant at $p < .01$.

Regarding colocalization of ADFP with the lipid droplets, P_r Li Pi Wm for control cells averaged 0.47, indicating a high degree of colocalization. For cells exposed to oleic acid, the mean value was somewhat elevated (0.58), but this degree of elevation did not meet the criteria of statistical significance in this multiple comparison experiment. The M_1 colocalization coefficients were similar for control vs. oleic acid-treated cells, and relatively high (mean values of 0.70 and 0.56, Figure 8E). In contrast M_2 averaged 0.14 for control vs. 0.77 for oleic acid-treated cells (Figure 8F), with very good consistency and this difference was statistical significance ($p < .01$) and yielded a Z' value of 0.61. The P_r Li Pi Wm data suggest that, in general, the lipid droplets and ADFP are colocalized in AML12 cells. However, the Mander's M_1 and M_2 coefficients provide insight into the situation. The relatively high values of the

M_1 coefficients, for example, indicate that for both control cells and oleic acid- treated cells, the majority of lipid staining intensity is correlated with the ADFP label. The M_2 values, however, suggest that under control conditions, much of the ADFP label is not associated with lipid staining; however, for cells treated with oleic acid, which feature more lipid droplets and more ADFP, the majority of the ADFP label intensity, is associated with the lipid stain.

Analysis of lipid droplets and ADFP in primary hepatocytes

A similar experiment was also performed with primary rat hepatocytes. Hepatocytes isolated from an adult rat were plated on a 96-well dish then exposed to 200 μM oleic acid overnight, then fixed and stained for lipid droplets and labeled for ADFP. More lipid droplets were found, per cell, for this cell type than for any of the hepatocyte-derived cell lines, and the droplets were well resolved by the imaging and by the automated algorithm. For the control cells, a relatively large number of small, weakly staining droplets were found (a mean of 101 per cell) (Figure 9A). ADFP was found both bordering the lipid droplets and, also, throughout the cytoplasm (Figure 9B). For cells exposed to oleic acid (Figure 9C and 9D), there was an average of 195 lipid droplets per cell (Figure 9E), and the total integrated intensity of the lipid droplets (TLL) was 14-fold higher (Figure 9F). In contrast, addition of oleic acid had only a mild effect on overall ADFP expression, as the area of the ADFP label was increased by just 11% (data not shown). The $P_r Li Pi Wm$ for the colocalization of the lipid droplets and ADFP was 0.60 for control cells and this increased to 0.66 for cells treated with oleic acid (Figure 9G). The M_1 colocalization coefficient averaged 0.82 for control cells and 0.70 for cells treated with oleic acid (not shown). The M_2 coefficient averaged 0.25 for control cells and was increased to 0.90 by treatment with oleic acid (Figure 9H). Thus, the colocalization constants calculated for lipid droplets and ADFP for the primary rat hepatocytes were very similar to those determined above for lipid droplets and ADFP in AML12 cells.

Analysis of lipid droplets HepG2 cells

HepG2 cells were also tested using the same methodology. However, HepG2 cells were somewhat 3-dimensional and had a tendency to clump. The HepG2 featured a large amount of lipid droplets in the control state (images not shown), with the lipid droplets representing 18.8% of the cell area. Addition of oleic acid to the HepG2 cells resulted in approximate 2-fold increases in the % of lipid droplet area, lipid droplet count, and TLL (data not shown).

Quantification of lipid droplets in HeLa and THP-1 cells

To test if CyteSeer® could quantify lipid droplet formation in HeLa (human cervical cancer-derived) and THP-1 cells (human macrophage-derived cells), the cells were treated with oleic acid and stained for neutral lipids via techniques identical to that used for the hepatocytes. In a time course experiment, HeLa cells were exposed to 150 μM oleic acid, for time periods of 1, 2, 4, 7, and 24 hrs. As quantified by the Lipid Droplet algorithm, control HeLa cells contained an average of 3.2 lipid droplets per cell, and this was increased to 11.3 lipid droplets per cell at the 7 hr time point (data not shown), which was the maximum number of droplet/cell that was observed for the experiment. The lipid droplet masks from HeLa cells were of high fidelity with regard to the lipid droplets (Figure 10A and 10B). For HeLa cells, one of the most consistent data parameters derived from the image set was the difference between the median pixel intensity of the lipid image at the lipid mask and the median pixel intensity of the lipid image at the cytoplasmic mask ($M_{pi Li Lm} - M_{pi Li Cm}$); this data parameter was significantly increased approximately 3-fold after just a 1 hr exposure to oleic acid, and increased 16-fold over the course of the experiment with a Z' value of 0.20 (Figure 10E).

THP-1 cells were proliferated in suspension, then differentiated to the macrophage phenotype by plating in the presence of 100 nM PMA. The cells were then exposed to different concentrations of oleic acid overnight. The Lipid Droplet algorithm readily identified lipid

droplets in the THP-1 cells (Figure 10C and 10D). Control cells featured an average of 4.0 lipid droplets/cell, and this was increased to 7.0 lipid droplets/cell by 150 μ M oleic acid (data not shown). For the THP-1 cells the data parameter corresponding to $M_{pi} Li Lm / M_{pi} Li Cm$ proved to be very consistent. For example, the lowest dose of oleic acid used in the experiment (19 μ M), elicited a 30% increase in this parameter that was highly statistically significant ($p < 0.001$) and $Z' = 0.69$ for the comparison between control cells and cells exposed to 300 μ M oleic acid (Figure 10F).

Discussion

The present study describes the development of high content/high throughput methodology for quantifying lipid droplets and lipid droplet-associated proteins in adipocytes and other cell types. Lipid droplets and associated proteins are an ideal subject for high content microscopy analysis, as the nuclei, droplets, and proteins are readily visualized in separate fluorescence channels in cells that have been cultured in a high throughput fashion.

To develop our methodology, we initially chose primary subcutaneous preadipocytes, harvested from adult humans via liposuction, as a model system. These were induced to produce lipid droplets by exposing the cells to rosi or a proprietary PPAR γ agonist. The preadipocytes adhered strongly to the multi-well dishes required for high throughput automated microscopy and were relatively flat, so that images could be captured at a single focal plane that visualized most of the lipid droplets with good focus.

The Lipid Droplet algorithm was designed to recognize the very small droplets that originate in subcutaneous preadipocytes during the beginning of the adipogenesis differentiation pathway induced by PPAR γ agonists. The algorithm quantified the effects of rosi with excellent consistency, yielding Z' values > 0.50 for a variety of data parameters. Thus, the assay is suitable for high throughput screening of chemical libraries, containing hundreds of thousands of compounds. Relatedly, the consistency of the analysis achieved by the algorithm also allowed subtle effects to be quantified, such as the positive effects of low concentrations (1 to 10 nM) of rosi on the lipid droplets in the human adipocytes. A benefit of developing methods to quantify the small droplets associated with the beginnings of adipogenesis, is that the algorithm also proved capable of quantifying lipid droplet formation in a variety of non-adipocytes, as shown here for hepatocytes, HeLa, and macrophages.

The use of colocalization analysis to quantify the association of proteins with lipid droplets provided a degree of quantification not typically considered in studies of PAT proteins. In adipocytes, cells were co-visualized for lipid and perilipin, a protein well known to be tightly associated with lipid droplets. Pearson's Correlation values determined between the lipid and protein images over the whole cell mask ($Pr Li PI Wm$) for perilipin vs. lipid droplets averaged approx. 0.37 to 0.48 in these experiments, indicating a large degree of colocalization. $Pr Li PI Wm$ is likely influenced by two relationships that have opposite effects on the coefficient: the considerable overlap in the lipid droplet and perilipin images within each cell represents a positive influence on $Pr Li PI Wm$. However, the inverse relationship between lipid intensity (brightest in the center) and perilipin intensity (dimmiest in the center) within each lipid droplet, acts to diminish $Pr Li PI Wm$. Thus, $Pr Li PI Wm$ values in the 0.35 to 0.50 range are likely to be as high as can be obtained for the PAT protein family for adipocytes imaged using the conventional fluorescence microscopy approach used in this study. In contrast, $Pr Li PI Wm$ values near zero were obtained for lipid droplets vs. the HSL label for adipocytes in control culture medium, indicating a random distribution between the lipid droplet stain and the HSL label.

The immunolabeling pattern for PKC in adipocytes yielded Pr Li Pi Wm values that were intermediate between perilipin and the HSL, suggesting some degree of association of PKC with the lipid droplets. Both PKC α and PKC β are present in adipocytes⁸⁶. Further, PKC isoforms regulate a variety of processes related to lipid droplet biology including expression of the PAT protein TIP47⁸⁷, adipocyte differentiation⁸⁸, magnolol-induced lipolysis⁸⁹ and cholesterol-induced targeting of caveolin to lipid droplets⁹⁰. The analysis described in the current study is the first, to our knowledge, to imply an association of PKC with lipid droplets in human subcutaneous adipocytes.

Colocalization analysis of ADFP and lipid droplets in hepatocytes provides insight into the likely mechanism via which ADFP participates in lipid droplet metabolism. In the absence of oleic acid, the AML12 cells displayed significant label for ADFP, even though lipid droplets were relatively sparse. The M₁ coefficient, which provided an index of the degree to which the lipid droplet fluorescent label was associated with ADFP label was high (e.g., approximately 0.7), indicating that most of the lipid that was associated with ADFP in the control cells. In contrast, the M₂ coefficient, which provides an index of the percentage of ADFP fluorescence intensity that is associated with lipid droplets, was low under control conditions indicating that much of the ADFP was independent of the relatively few and small lipid droplets found in the absence of oleic acid. When oleic acid was added, yielding larger and more numerous droplets, the M₂ coefficient, strongly increased. This is the relationship that would be expected for a protein that is present prior to lipid droplet formation, and which migrates to the surface of droplets at early stages of droplet formation, as has been previously observed for ADFP^{30, 91}.

Of the hepatocyte-derived cell lines considered in this study, under control conditions, AML12 cells expressed the fewest and smallest droplets, followed by the Huh-7 cells, and HepG2 cells. This is consistent with the origin of each cell line. AML12 cells were derived from a transgenic mouse overexpressing TGF α ⁹² and are mitotic, but retain many features of normal hepatocytes. Both Huh-7⁹³ and HepG2⁹⁴ cells, however, were derived from hepatocellular carcinomas. Lipid droplets are common in hepatocellular carcinomas as the enzymatic pathways responsible for lipid droplet formation are upregulated in this cancer type⁹⁵; furthermore, fatty liver disease and Metabolic Syndrome are risk factors for hepatocellular carcinoma⁹⁶. Thus, the AML12 cells likely represent a model for “normal” liver, whereas Huh-7 and HepG2 might best be considered models for fatty liver. Our results suggest that AML12 and Huh-7 are readily suitable for high throughput/high content-based screening strategies to screen chemical or genomic libraries for probes or genes that increase or inhibit lipid droplet formation in the context of the hepatocyte. Primary rat hepatocytes also responded to oleic acid with a very strong increase in lipid labeling. The colocalization analysis of lipid droplets and ADFP label yielded similar results for the primary hepatocytes and AML12 cells, which is further evidence of the near-normal phenotype of the AML12 cell line.

The results with the macrophages suggest that this methodology can be used to screen macrophage-type cells for probes or genes that influence lipid droplet metabolism in the context of coronary artery disease^{21, 97} and tuberculosis^{23, 24}, two diseases in which “foam” cell (macrophages loaded with lipid droplets), play a strong role in the respective etiologies.

Image based high content screens designed to probe lipid droplet metabolic pathways via use of siRNA libraries and related techniques have recently been performed for *Drosophila* S2 and K_{C167} cell lines and have identified Coat Protein Complex I (COPI) proteins as important mediators of lipid droplet formation^{98, 99}; furthermore, the relevance of these findings to mammalian cells was confirmed with AML12 and 3T3L1 cells⁹⁹. Also, image based analysis of lipid droplets in yeast deletion strains has identified a lipid droplet regulating function for seipin, a protein mutated in patients with Berardinelli-Seip Congenital Lipodystrophy, a

condition in which adipose tissue is severely reduced 100. In these previous studies, digital images were acquired from the relevant cell models, and the images laboriously analyzed by visual inspection, or by custom-designed image analysis algorithms. The Java-encoded algorithms used in this study are portable to a variety of computer operating systems (PC, McIntosh, Linux), can be operated in a “batch” mode to analyze images acquired from hundreds of multiple-well dishes, and includes the ability to quantify colocalization of lipid droplets with proteins or any cellular structure that can be visualized by fluorescent labeling techniques. Future directions will include development of algorithms to quantify the spatial distribution of droplets within the cell and the analysis of lipid droplets in tissue sections.

Acknowledgments

We thank Dr. Brian A. Naughton (RegeneMed Inc.) for the generous gift of primary rat hepatocytes. We thank Dr. Constantine Londos for the generous gift of the anti-ADFP antibody. This research was supported, in part, by National Institutes of Health grants 1R43DK074333 (PMM).

References

- Haffner SM. Relationship of metabolic risk factors and development of cardiovascular disease and diabetes. *Obesity (Silver Spring)* 2006 Jun;14:121S–127S. [PubMed: 16931493]
- Hensrud DD, Klein S. Extreme obesity: a new medical crisis in the United States. *Mayo Clin Proc* 2006 Oct;81(10 Suppl):S5–S10. [PubMed: 17036573]
- Francischetti EA, Genelhu VA. Obesity-hypertension: an ongoing pandemic. *Int J Clin Pract* 2007 Feb;61(2):269–280. [PubMed: 17263714]
- Hill JO, Peters JC, Wyatt HR. The role of public policy in treating the epidemic of global obesity. *Clin Pharmacol Ther* 2007 May;81(5):772–775. [PubMed: 17314927]
- Dehghan M, Akhtar-Danesh N, Merchant AT. Childhood obesity, prevalence and prevention. *Nutr J* 2005;4:24. [PubMed: 16138930]
- Orio F Jr, Palomba S, Cascella T, Savastano S, Lombardi G, Colao A. Cardiovascular complications of obesity in adolescents. *J Endocrinol Invest* 2007 Jan;30(1):70–80. [PubMed: 17318026]
- Wyatt SB, Winters KP, Dubbert PM. Overweight and obesity: prevalence, consequences, and causes of a growing public health problem. *Am J Med Sci* 2006 Apr;331(4):166–174. [PubMed: 16617231]
- Neuschwander-Tetri BA. Fatty liver and the metabolic syndrome. *Curr Opin Gastroenterol* 2007 Mar;23(2):193–198. [PubMed: 17268250]
- Saadeh S. Nonalcoholic Fatty liver disease and obesity. *Nutr Clin Pract* 2007 Feb;22(1):1–10. [PubMed: 17242448]
- Reddy JK, Rao MS. Lipid metabolism and Liver inflammation. II. Fatty liver disease and fatty acid oxidation. *Am J Physiol Gastrointest Liver Physiol* 2006 May;290(5):G852–G858. [PubMed: 16603729]
- Moscatiello S, Manini R, Marchesini G. Diabetes and liver disease: an ominous association. *Nutr Metab Cardiovasc Dis* 2007 Jan;17(1):63–70. [PubMed: 17164082]
- Targher G, Bertolini L, Padovani R, et al. Prevalence of nonalcoholic fatty liver disease and its association with cardiovascular disease among type 2 diabetic patients. *Diabetes Care* 2007 May;30(5):1212–1218. [PubMed: 17277038]
- Bondini S, Younossi ZM. Non-alcoholic fatty liver disease and hepatitis C infection. *Minerva Gastroenterol Dietol* 2006 Jun;52(2):135–143. [PubMed: 16557185]
- Boulant S, Targett-Adams P, McLauchlan J. Disrupting the association of hepatitis C virus core protein with lipid droplets correlates with a loss in production of infectious virus. *J Gen Virol* 2007 Aug;88(Pt 8):2204–2213. [PubMed: 17622624]
- Schrauwen-Hinderling VB, Hesselink MK, Schrauwen P, Kooi ME. Intramyocellular lipid content in human skeletal muscle. *Obesity (Silver Spring)* 2006 Mar;14(3):357–367. [PubMed: 16648604]
- Sharma S, Adroque JV, Golfman L, et al. Intramyocardial lipid accumulation in the failing human heart resembles the lipotoxic rat heart. *FASEB J* 2004 Nov;18(14):1692–1700. [PubMed: 15522914]

17. Christoffersen C, Bollano E, Lindegaard ML, et al. Cardiac lipid accumulation associated with diastolic dysfunction in obese mice. *Endocrinology* 2003 Aug;144(8):3483–3490. [PubMed: 12865329]
18. Ueno M, Suzuki J, Zenimaru Y, et al. Cardiac overexpression of hormone-sensitive lipase inhibits myocardial steatosis and fibrosis in streptozotocin diabetic mice. *Am J Physiol Endocrinol Metab* 2008 Jun;294(6):E1109–E1118. [PubMed: 18413675]
19. Man ZW, Zhu M, Noma Y, et al. Impaired beta-cell function and deposition of fat droplets in the pancreas as a consequence of hypertriglyceridemia in OLETF rat, a model of spontaneous NIDDM. *Diabetes* 1997 Nov;46(11):1718–1724. [PubMed: 9356017]
20. Fex M, Nitert MD, Wierup N, Sundler F, Ling C, Mulder H. Enhanced mitochondrial metabolism may account for the adaptation to insulin resistance in islets from C57BL/6J mice fed a high-fat diet. *Diabetologia* 2007 Jan;50(1):74–83. [PubMed: 17093947]
21. Choudhury RP, Lee JM, Greaves DR. Mechanisms of disease: macrophage-derived foam cells emerging as therapeutic targets in atherosclerosis. *Nat Clin Pract Cardiovasc Med* 2005 Jun;2(6):309–315. [PubMed: 16265535]
22. Larigauderie G, Cuaz-Perolin C, Younes AB, et al. Adipophilin increases triglyceride storage in human macrophages by stimulation of biosynthesis and inhibition of beta-oxidation. *FEBS J* 2006 Aug;273(15):3498–3510. [PubMed: 16884492]
23. Ordway D, Henaio-Tamayo M, Orme IM, Gonzalez-Juarrero M. Foamy macrophages within lung granulomas of mice infected with *Mycobacterium tuberculosis* express molecules characteristic of dendritic cells and antiapoptotic markers of the TNF receptor-associated factor family. *J Immunol* 2005 Sep 15;175(6):3873–3881. [PubMed: 16148133]
24. D'Avila H, Melo RC, Parreira GG, Werneck-Barroso E, Castro-Faria-Neto HC, Bozza PT. *Mycobacterium bovis* bacillus Calmette-Guerin induces TLR2-mediated formation of lipid bodies: intracellular domains for eicosanoid synthesis in vivo. *J Immunol* 2006 Mar 1;176(5):3087–3097. [PubMed: 16493068]
25. Tarnopolsky MA, Rennie CD, Robertshaw HA, Fedak-Tarnopolsky SN, Devries MC, Hamadeh MJ. Influence of endurance exercise training and sex on intramyocellular lipid and mitochondrial ultrastructure, substrate use, and mitochondrial enzyme activity. *Am J Physiol Regul Integr Comp Physiol* 2007 Mar;292(3):R1271–R1278. [PubMed: 17095651]
26. Weinberg JM. Lipotoxicity. *Kidney Int* 2006 Nov;70(9):1560–1566. [PubMed: 16955100]
27. Kusunoki J, Kanatani A, Moller DE. Modulation of fatty acid metabolism as a potential approach to the treatment of obesity and the metabolic syndrome. *Endocrine* 2006 Feb;29(1):91–100. [PubMed: 16622296]
28. Ghosh S, Rodrigues B. Cardiac cell death in early diabetes and its modulation by dietary fatty acids. *Biochim Biophys Acta* 2006 Oct;1761(10):1148–1162. [PubMed: 16997625]
29. Robenek MJ, Severs NJ, Schlattmann K, et al. Lipids partition caveolin-1 from ER membranes into lipid droplets: updating the model of lipid droplet biogenesis. *FASEB J* 2004 May;18(7):866–868. [PubMed: 15001554]
30. Wolins NE, Quaynor BK, Skinner JR, Schoenfish MJ, Tzekov A, Bickel PE. S3-12, Adipophilin, and TIP47 package lipid in adipocytes. *J Biol Chem* 2005 May 13;280(19):19146–19155. [PubMed: 15731108]
31. Wolins NE, Brasaemle DL, Bickel PE. A proposed model of fat packaging by exchangeable lipid droplet proteins. *FEBS Lett* 2006 Oct 9;580(23):5484–5491. [PubMed: 16962104]
32. Song H, O'Connor KC, Papadopoulos KD, Jansen DA. Differentiation kinetics of in vitro 3T3-L1 preadipocyte cultures. *Tissue Eng* 2002 Dec;8(6):1071–1081. [PubMed: 12542952]
33. Hickenbottom SJ, Kimmel AR, Londos C, Hurley JH. Structure of a lipid droplet protein; the PAT family member TIP47. *Structure* 2004 Jul;12(7):1199–1207. [PubMed: 15242596]
34. Chang BH, Li L, Paul A, et al. Protection against fatty liver but normal adipogenesis in mice lacking adipose differentiation-related protein. *Mol Cell Biol* 2006 Feb;26(3):1063–1076. [PubMed: 16428458]
35. Motomura W, Inoue M, Ohtake T, et al. Up-regulation of ADRP in fatty liver in human and liver steatosis in mice fed with high fat diet. *Biochem Biophys Res Commun* 2006 Feb 24;340(4):1111–1118. [PubMed: 16403437]

36. Chang BH, Chan L. Regulation of Triglyceride Metabolism. III. Emerging role of lipid droplet protein ADFP in health and disease. *Am J Physiol Gastrointest Liver Physiol* 2007 Jun;292(6):G1465–G1468. [PubMed: 17194897]
37. Shen WJ, Patel S, Yu Z, Jue D, Kraemer FB. Effects of rosiglitazone and high fat diet on lipase/esterase expression in adipose tissue. *Biochim Biophys Acta* 2007 Feb;1771(2):177–184. [PubMed: 17215164]
38. Jocken JW, Langin D, Smit E, et al. Adipose triglyceride lipase and hormone-sensitive lipase protein expression is decreased in the obese insulin-resistant state. *J Clin Endocrinol Metab* 2007 Jun;92(6):2292–2299. [PubMed: 17356053]
39. Jaworski K, Sarkadi-Nagy E, Duncan RE, Ahmadian M, Sul HS. Regulation of triglyceride metabolism. IV. Hormonal regulation of lipolysis in adipose tissue. *Am J Physiol Gastrointest Liver Physiol* 2007 Jul;293(1):G1–G4. [PubMed: 17218471]
40. Gronke S, Mildner A, Fellert S, et al. Brummer lipase is an evolutionary conserved fat storage regulator in *Drosophila*. *Cell Metab* 2005 May;1(5):323–330. [PubMed: 16054079]
41. Saha PK, Kojima H, Martinez-Botia J, Sunehag AL, Chan L. Metabolic adaptations in the absence of perilipin: increased beta-oxidation and decreased hepatic glucose production associated with peripheral insulin resistance but normal glucose tolerance in perilipin-null mice. *J Biol Chem* 2004 Aug 20;279(34):35150–35158. [PubMed: 15197189]
42. Londos C, Sztalryd C, Tansey JT, Kimmel AR. Role of PAT proteins in lipid metabolism. *Biochimie* 2005 Jan;87(1):45–49. [PubMed: 15733736]
43. Londos C, Brasaemle DL, Schultz CJ, Segrest JP, Kimmel AR. Perilipins, ADRP, and other proteins that associate with intracellular neutral lipid droplets in animal cells. *Semin Cell Dev Biol* 1999 Feb;10(1):51–58. [PubMed: 10355028]
44. Clifford GM, Londos C, Kraemer FB, Vernon RG, Yeaman SJ. Translocation of hormone-sensitive lipase and perilipin upon lipolytic stimulation of rat adipocytes. *J Biol Chem* 2000 Feb 18;275(7):5011–5015. [PubMed: 10671541]
45. Chung S, Brown JM, Sandberg MB, McIntosh M. Trans-10,cis-12 CLA increases adipocyte lipolysis and alters lipid droplet-associated proteins: role of mTOR and ERK signaling. *J Lipid Res* 2005 May;46(5):885–895. [PubMed: 15716587]
46. Brasaemle DL, Levin DM, Adler-Wailes DC, Londos C. The lipolytic stimulation of 3T3-L1 adipocytes promotes the translocation of hormone-sensitive lipase to the surfaces of lipid storage droplets. *Biochim Biophys Acta* 2000 Jan 17;1483(2):251–262. [PubMed: 10634941]
47. Miyoshi H, Perfield JW 2nd, Souza SC, et al. Control of adipose triglyceride lipase action by serine 517 of perilipin A globally regulates protein kinase A-stimulated lipolysis in adipocytes. *J Biol Chem* 2007 Jan 12;282(2):996–1002. [PubMed: 17114792]
48. Athenstaedt K, Zweytick D, Jandrositz A, Kohlwein SD, Daum G. Identification and characterization of major lipid particle proteins of the yeast *Saccharomyces cerevisiae*. *J Bacteriol* 1999 Oct;181(20):6441–6448. [PubMed: 10515935]
49. Brasaemle DL, Dolios G, Shapiro L, Wang R. Proteomic analysis of proteins associated with lipid droplets of basal and lipolytically stimulated 3T3-L1 adipocytes. *J Biol Chem* 2004 Nov 5;279(45):46835–46842. [PubMed: 15337753]
50. Beller M, Riedel D, Jansch L, et al. Characterization of the *Drosophila* lipid droplet subproteome. *Mol Cell Proteomics* 2006 Jun;5(6):1082–1094. [PubMed: 16543254]
51. Turro S, Ingelmo-Torres M, Estanyol JM, et al. Identification and characterization of associated with lipid droplet protein 1: A novel membrane-associated protein that resides on hepatic lipid droplets. *Traffic* 2006 Sep;7(9):1254–1269. [PubMed: 17004324]
52. Aza-Blanc P, Cooper CL, Wagner K, Batalov S, Deveraux QL, Cooke MP. Identification of modulators of TRAIL-induced apoptosis via RNAi-based phenotypic screening. *Mol Cell* 2003 Sep;12(3):627–637. [PubMed: 14527409]
53. Berno V, Hinojos CA, Amazit L, Szafran AT, Mancini MA. High-resolution, high-throughput microscopy analyses of nuclear receptor and coregulator function. *Methods Enzymol* 2006;414:188–210. [PubMed: 17110193]
54. Bettencourt-Dias M, Giet R, Sinka R, et al. Genome-wide survey of protein kinases required for cell cycle progression. *Nature* 2004 Dec 23;432(7020):980–987. [PubMed: 15616552]

55. Carpenter AE, Sabatini DM. Systematic genome-wide screens of gene function. *Nat Rev Genet* 2004 Jan;5(1):11–22. [PubMed: 14708012]
56. Cho CY, Koo SH, Wang Y, et al. Identification of the tyrosine phosphatase PTP-MEG2 as an antagonist of hepatic insulin signaling. *Cell Metab* 2006 May;3(5):367–378. [PubMed: 16679294]
57. Harada JN, Bower KE, Orth AP, et al. Identification of novel mammalian growth regulatory factors by genome-scale quantitative image analysis. *Genome Res* 2005 Aug;15(8):1136–1144. [PubMed: 16024821]
58. Huang Q, Raya A, DeJesus P, et al. Identification of p53 regulators by genome-wide functional analysis. *Proc Natl Acad Sci U S A* 2004 Mar 9;101(10):3456–3461. [PubMed: 14990790]
59. Iourgenko V, Zhang W, Mickanin C, et al. Identification of a family of cAMP response element-binding protein coactivators by genome-scale functional analysis in mammalian cells. *Proc Natl Acad Sci U S A* 2003 Oct 14;100(21):12147–12152. [PubMed: 14506290]
60. Marcelli M, Stenoien DL, Szafran AT, et al. Quantifying effects of ligands on androgen receptor nuclear translocation, intranuclear dynamics, and solubility. *J Cell Biochem* 2006 Jul 1;98(4):770–788. [PubMed: 16440331]
61. Mukherji M, Bell R, Supekova L, et al. Genome-wide functional analysis of human cell-cycle regulators. *Proc Natl Acad Sci U S A* 2006 Oct 3;103(40):14819–14824. [PubMed: 17001007]
62. Rines DR, Tu B, Miraglia L, et al. High-content screening of functional genomic libraries. *Methods Enzymol* 2006;414:530–565. [PubMed: 17110210]
63. Sharp ZD, Mancini MG, Hinojos CA, et al. Estrogen-receptor-alpha exchange and chromatin dynamics are ligand- and domain-dependent. *J Cell Sci* 2006 Oct 1;119(Pt 19):4101–4116. [PubMed: 16968748]
64. Zheng L, Liu J, Batalov S, et al. An approach to genomewide screens of expressed small interfering RNAs in mammalian cells. *Proc Natl Acad Sci U S A* 2004 Jan 6;101(1):135–140. [PubMed: 14688408]
65. Dragunow M. High-content analysis in neuroscience. *Nat Rev Neurosci* 2008 Oct;9(10):779–788. [PubMed: 18784656]
66. Haney SA, LaPan P, Pan J, Zhang J. High-content screening moves to the front of the line. *Drug Discov Today* 2006 Oct;11(19–20):889–894. [PubMed: 16997138]
67. Giuliano KA, Johnston PA, Gough A, Taylor DL. Systems cell biology based on high-content screening. *Methods Enzymol* 2006;414:601–619. [PubMed: 17110213]
68. Nicholson RL, Welch M, Ladlow M, Spring DR. Small-molecule screening: advances in microarraying and cell-imaging technologies. *ACS Chem Biol* 2007 Jan 23;2(1):24–30. [PubMed: 17243780]
69. Morelock MM, Hunter EA, Moran TJ, et al. Statistics of assay validation in high throughput cell imaging of nuclear factor kappaB nuclear translocation. *Assay Drug Dev Technol* 2005 Oct;3(5):483–499. [PubMed: 16305306]
70. Prigozhina NL, Zhong L, Hunter EA, et al. Plasma membrane assays and three-compartment image cytometry for high content screening. *Assay Drug Dev Technol* 2007 Feb;5(1):29–48. [PubMed: 17355198]
71. Carpenter AE, Jones TR, Lamprecht MR, et al. CellProfiler: image analysis software for identifying and quantifying cell phenotypes. *Genome Biol* 2006 Oct 31;7(10):R100. [PubMed: 17076895]
72. Chen X, Murphy RF. Objective clustering of proteins based on subcellular location patterns. *J Biomed Biotechnol* 2005 Jun 30;2005(2):87–95. [PubMed: 16046813]
73. Hunter EA, Callaway WS, Price JH. Software Framework for Scanning Cytometry. *Proc. Of SPIE, Optical Diagnostics of Living Cells III* 2000;3921:41–52.
74. Price JH, Goodacre A, Hahn K, et al. Advances in molecular labeling, high throughput imaging and machine intelligence portend powerful functional cellular biochemistry tools. *J Cell Biochem Suppl* 2002;39:194–210. [PubMed: 12552619]
75. Roques EJ, Murphy RF. Objective evaluation of differences in protein subcellular distribution. *Traffic* 2002 Jan;3(1):61–65. [PubMed: 11872143]
76. Shen F, Hodgson L, Rabinovich A, Pertz O, Hahn K, Price JH. Functional proteomics for cell migration. *Cytometry A* 2006 Jul;69(7):563–572. [PubMed: 16752422]

77. Shen F, Price JH. Toward complete laser ablation of melanoma contaminant cells in a co-culture outgrowth model via image cytometry. *Cytometry A* 2006 Jul;69(7):573–581. [PubMed: 16807895]
78. Tarnok A. Slide-based cytometry for cytomics--a minireview. *Cytometry A* 2006 Jul;69(7):555–562. [PubMed: 16807894]
79. Carpenter AE. Software opens the door to quantitative imaging. *Nat Methods* 2007 Feb;4(2):120–121. [PubMed: 17264858]
80. Manders EMM, Verbeek FJ, Aten JA. Measurement of co-localization of objects in dual-colour confocal images. *Journal of Microscopy* 1993;169:375–382.
81. Zhang JH, Chung TD, Oldenburg KR. A Simple Statistical Parameter for Use in Evaluation and Validation of High Throughput Screening Assays. *J Biomol Screen* 1999;4(2):67–73. [PubMed: 10838414]
82. Russ JC. *The Image Processing Handbook*. CRC Press, Boca Raton. 1992
83. Mikic I, Planey S, Zhang J, et al. A live cell, image-based approach to understanding the enzymology and pharmacology of 2-bromopalmitate and palmitoylation. *Methods Enzymol* 2006;414:150–187. [PubMed: 17110192]
84. Hunter EA, McDonough PM, Mikic I, Price JH, Hunter EA, McDonough PM, Mikic I, Price JH, Hunter EA, McDonough PM, Mikic I, Price JH. Vala Sciences, Inc., assignee. System, Method and Kit for Processing a Magnified Image of Biological Material to Identify Components of a Biological Object. PCT Patent Application WO/2007/061971. 2005 November 21;
85. Xu G, Sztalryd C, Londos C. Degradation of perilipin is mediated through ubiquitination-proteasome pathway. *Biochim Biophys Acta* 2006 Jan;1761(1):83–90. [PubMed: 16448845]
86. Nakamura J. Protein kinase Cbeta1 interacts with the beta1-adrenergic signaling pathway to attenuate lipolysis in rat adipocytes. *Biochim Biophys Acta* 2008 May;1781(5):277–281. [PubMed: 18440322]
87. Than NG, Sumegi B, Bellyei S, et al. Lipid droplet and milk lipid globule membrane associated placental protein 17b (PP17b) is involved in apoptotic and differentiation processes of human epithelial cervical carcinoma cells. *Eur J Biochem* 2003 Mar;270(6):1176–1188. [PubMed: 12631276]
88. Hauner H, Petruschke T, Gries FA. Endothelin-1 inhibits the adipose differentiation of cultured human adipocyte precursor cells. *Metabolism* 1994 Feb;43(2):227–232. [PubMed: 8121307]
89. Huang SH, Shen WJ, Yeo HL, Wang SM. Signaling pathway of magnolol-stimulated lipolysis in sterol ester-loaded 3T3-L1 preadipocytes. *J Cell Biochem* 2004 Apr 1;91(5):1021–1029. [PubMed: 15034936]
90. Le Lay S, Hajduch E, Lindsay MR, et al. Cholesterol-induced caveolin targeting to lipid droplets in adipocytes: a role for caveolar endocytosis. *Traffic* 2006 May;7(5):549–561. [PubMed: 16643278]
91. Listenberger LL, Ostermeyer-Fay AG, Goldberg EB, Brown WJ, Brown DA. Adipocyte differentiation-related protein reduces the lipid droplet association of adipose triglyceride lipase and slows triacylglycerol turnover. *J Lipid Res* 2007 Dec;48(12):2751–2761. [PubMed: 17872589]
92. Wu JC, Merlino G, Fausto N. Establishment and characterization of differentiated, nontransformed hepatocyte cell lines derived from mice transgenic for transforming growth factor alpha. *Proc Natl Acad Sci U S A* 1994 Jan 18;91(2):674–678. [PubMed: 7904757]
93. Nakabayashi H, Taketa K, Miyano K, Yamane T, Sato J. Growth of human hepatoma cells lines with differentiated functions in chemically defined medium. *Cancer Res* 1982 Sep;42(9):3858–3863. [PubMed: 6286115]
94. Schwartz AL, Fridovich SE, Knowles BB, Lodish HF. Characterization of the asialoglycoprotein receptor in a continuous hepatoma line. *J Biol Chem* 1981 Sep 10;256(17):8878–8881. [PubMed: 6267054]
95. Yahagi N, Shimano H, Hasegawa K, et al. Co-ordinate activation of lipogenic enzymes in hepatocellular carcinoma. *Eur J Cancer* 2005 Jun;41(9):1316–1322. [PubMed: 15869874]
96. de Alwis NM, Day CP. Non-alcoholic fatty liver disease: the mist gradually clears. *J Hepatol* 2008;48(1):S104–S112. [PubMed: 18304679]
97. Pennings M, Meurs I, Ye D, et al. Regulation of cholesterol homeostasis in macrophages and consequences for atherosclerotic lesion development. *FEBS Lett* 2006 Oct 9;580(23):5588–5596. [PubMed: 16935283]

98. Guo Y, Walther TC, Rao M, et al. Functional genomic screen reveals genes involved in lipid-droplet formation and utilization. *Nature* 2008 May 29;453(7195):657–661. [PubMed: 18408709]
99. Beller M, Sztalryd C, Southall N, et al. COPI complex is a regulator of lipid homeostasis. *PLoS Biol* 2008 Nov 25;6(11):e292. [PubMed: 19067489]
100. Szymanski KM, Binns D, Bartz R, et al. The lipodystrophy protein seipin is found at endoplasmic reticulum lipid droplet junctions and is important for droplet morphology. *Proc Natl Acad Sci U S A* 2007 Dec 26;104(52):20890–20895. [PubMed: 18093937]

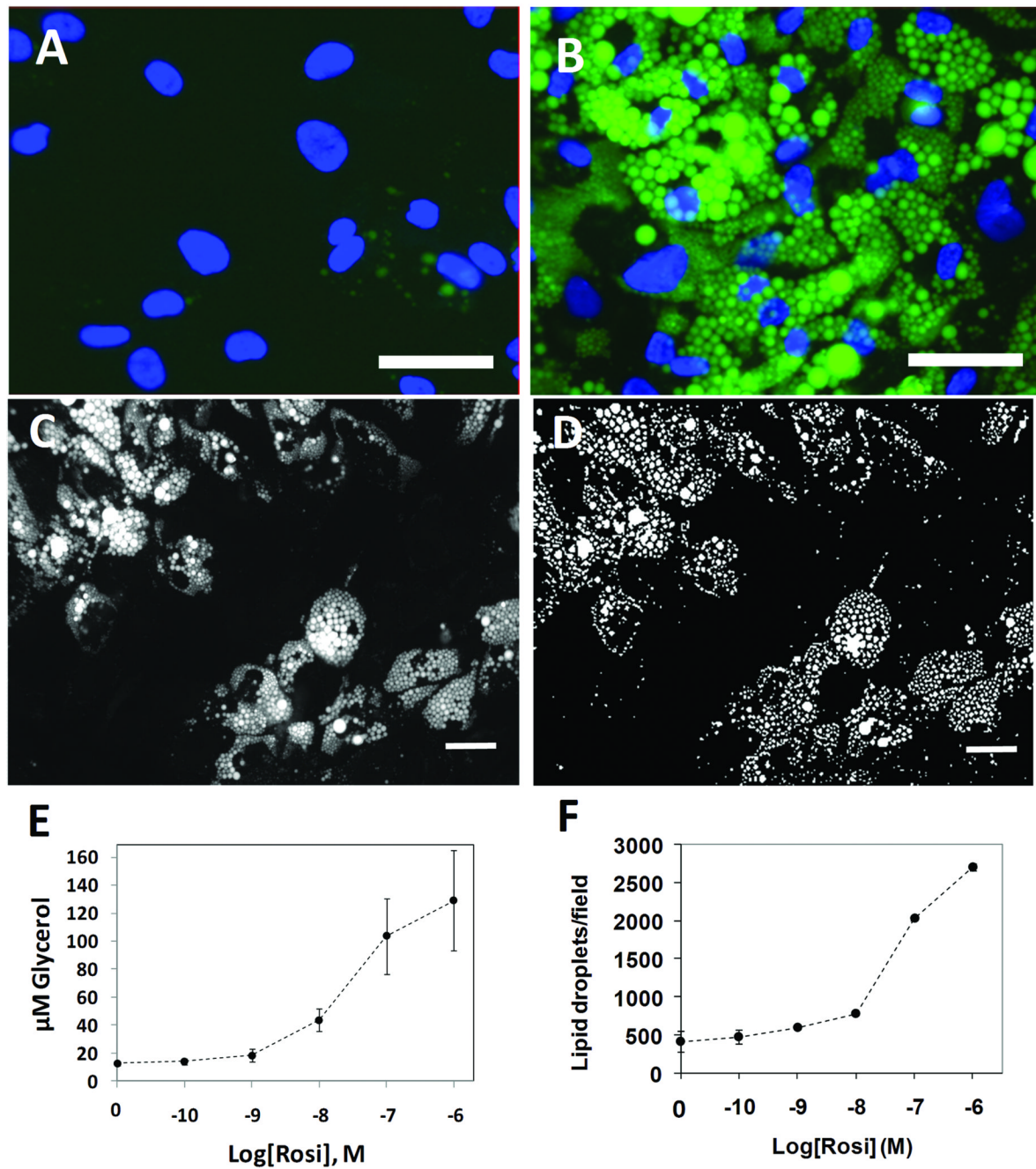


Figure 1. Development of the Lipid Droplet algorithm

Human primary preadipocytes were cultured in 96-well dishes in the absence or presence of 1 μM rosiglitazone for 14 days; the cells were then fixed, permeabilized and labeled for nuclei and lipid droplets using Vala's Lipid Droplet reagent kit, then imaged using a Beckman IC 100 Image Cytometer outfitted with a 40X objective. A, Control cells cultured in the absence of rosiglitazone; nuclei are blue and lipid droplets are green. B, Cells exposed to 1 μM rosiglitazone. C, Gray scale image of the lipid droplet image obtained from rosi-treated cells. D, A binary mask is shown, derived from C, in which the individual lipid droplets are identified. E, The effect of rosi on triglyceride content is shown (each symbol is the mean \pm SD, n=8 wells).

F, The effect of rosi on lipid droplets/field of view is shown, as quantified by the Lipid Droplet algorithm (each symbol is the Mean \pm range, n= 2 wells). Scale bars are 50 μ m.

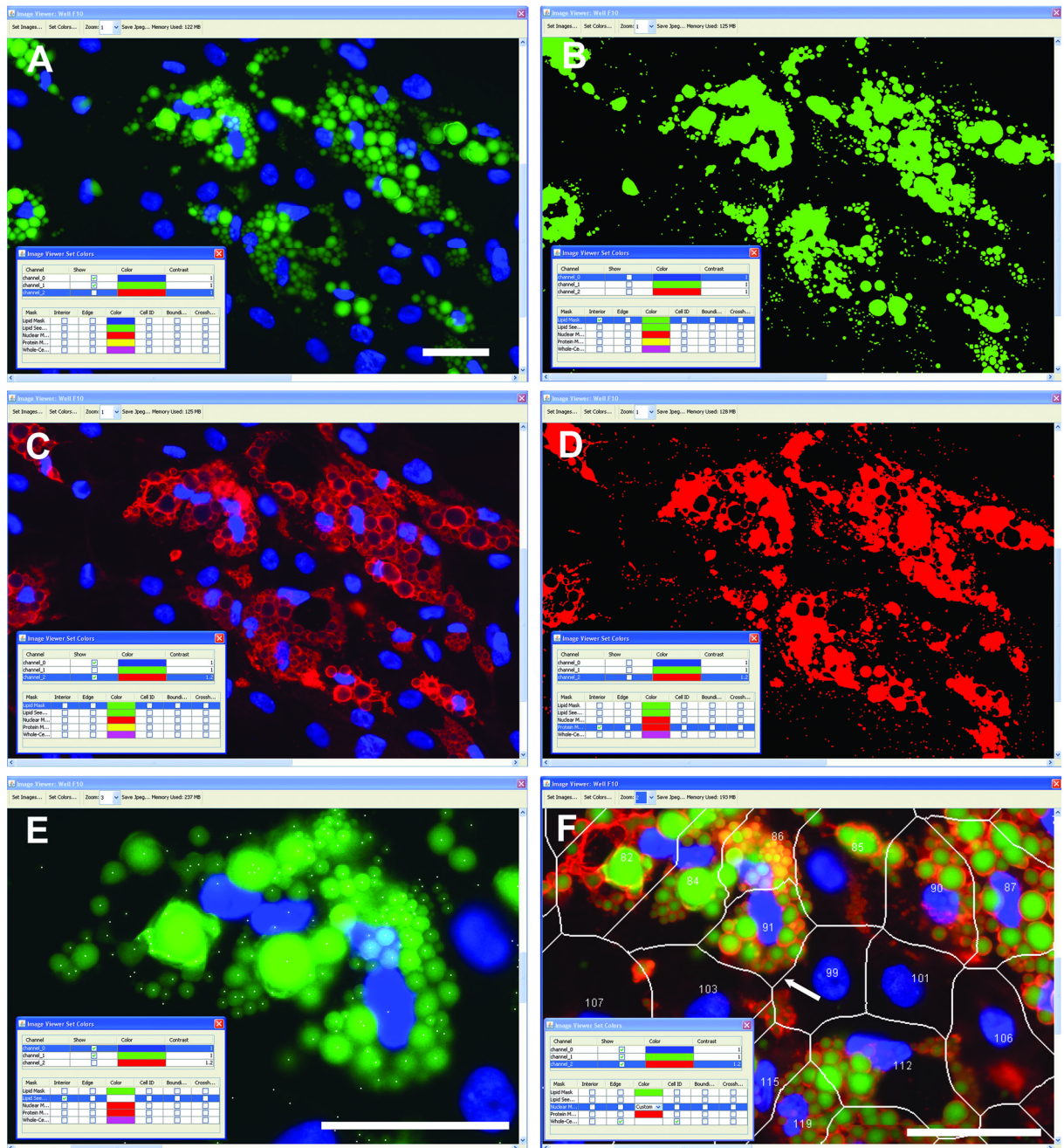


Figure 2. Incorporation of the Lipid Droplet, Perlipin, and Membrane Tessellation algorithms into CyteSeer®

Human preadipocytes were exposed to 1 μM of a proprietary PPAR γ agonist (Zen-Bio) for 19 days, then stained for nuclei, lipid, and perlipin and imaged with a 40X objective. A, A representative field of view is shown, featuring the lipid (green) and nuclear (blue) image channels. B, The Lipid Mask (green) derived by the Lipid Droplet algorithm encoded within CyteSeer® is shown. C, The perlipin image is shown (red). D, The Protein Mask derived by the Colocalization algorithm is shown. E, The lipid and nuclear images are shown at a higher magnification, and the lipid droplet “seed mask” is overlaid (white spots). F, The lipid, nuclear, and perlipin images are shown along with the cell boundary mask and cell identification

numbers; the white arrow identifies a boundary between a cell that features extensive lipid droplets (Cell #91) vs. a cell with few droplets (Cell #99). All panels were derived from the same field of view and represent screenshots from CyteSeer®'s Image Viewer. The scale bar is 50 μm .

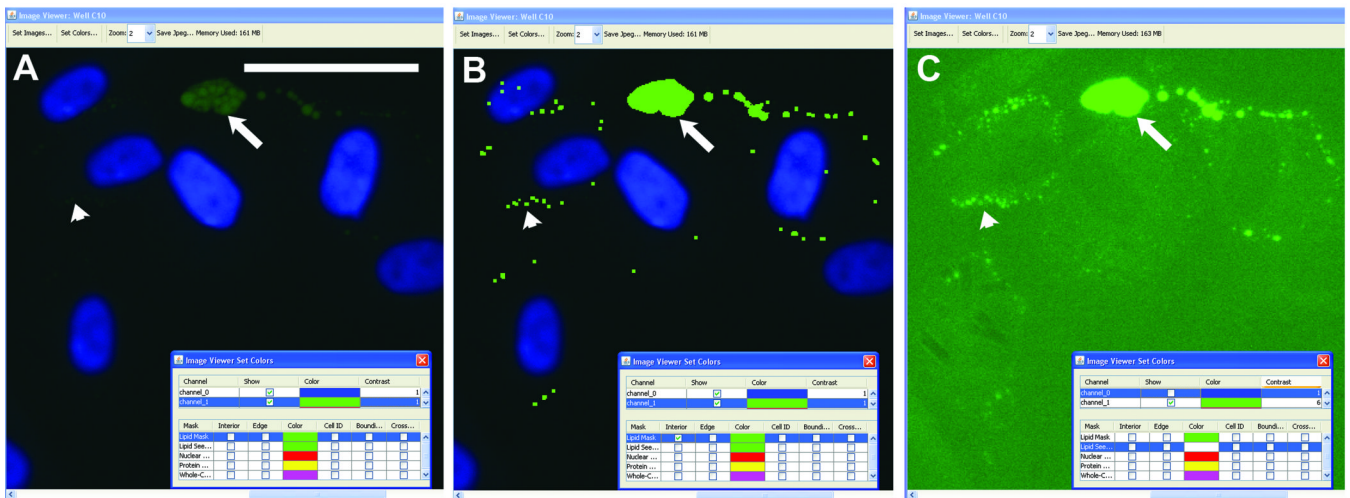


Figure 3. Sensitivity of the Lipid Droplet algorithm

Human preadipocytes were exposed to 0.33 nM rosiglitazone for 9 days, then labeled for nuclei and lipid droplets and imaged using a 40X objective. A, A field of view is shown in which the brightness of the image is shown at default levels (contrast = 1 in CyteSeer®'s Image Viewer). B, The same field of view is shown visualized for nuclei and the lipid droplet mask. C, The same field of view is shown visualized for lipid droplets at contrast = 6 (pixel intensities multiplied by 6-fold and clipped at 255 for the 8-bit image). The arrow denotes a cluster of relatively bright lipid droplets, whereas the arrowhead denotes an example of lipid droplets, identified by CyteSeer®, which are only visible in C. The scale bar is 50 μm .

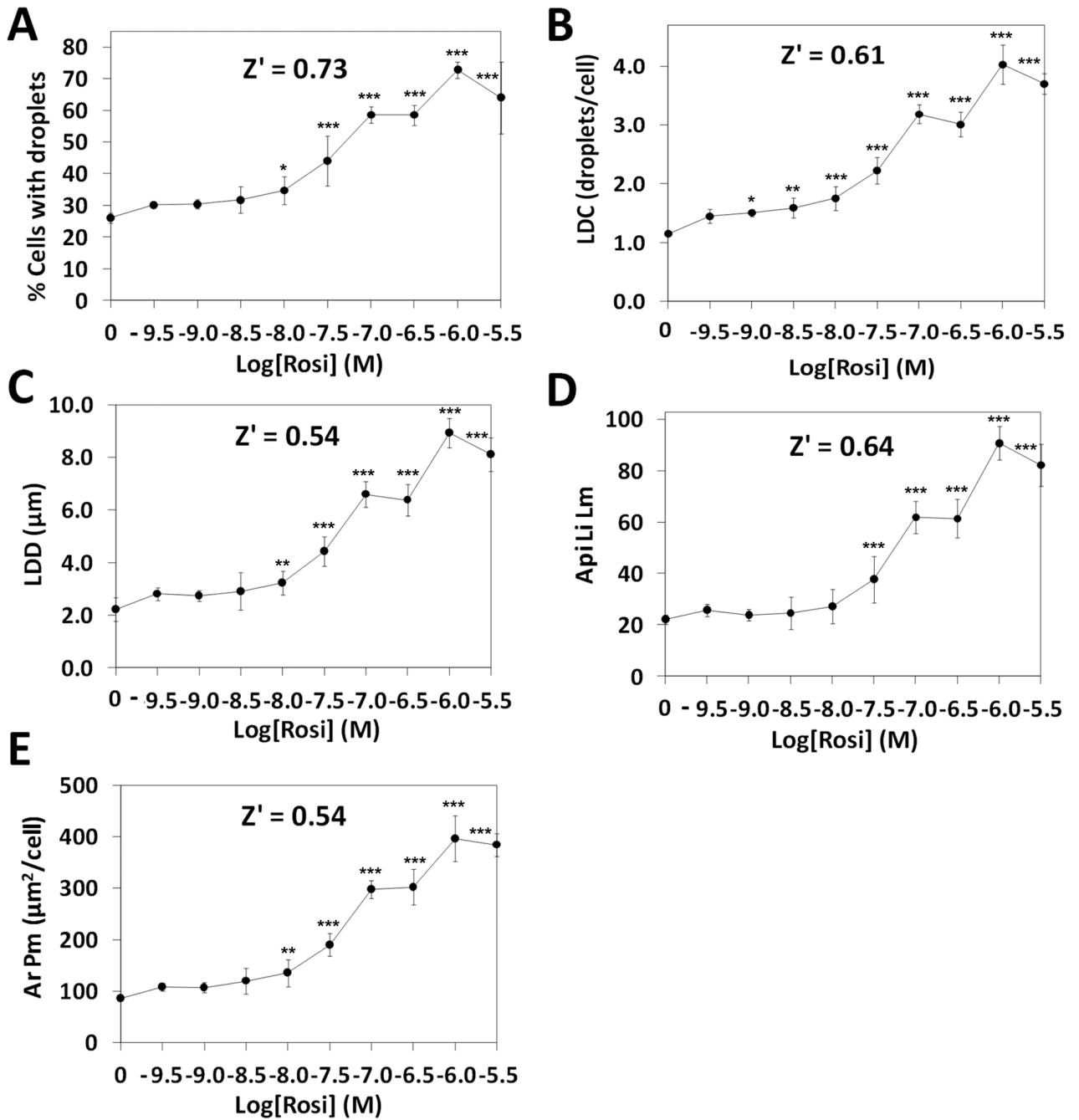


Figure 4. Quantification of lipid droplets and perilipin in primary human preadipocytes exposed to rosi

Cells were exposed to rosi for 9 days, then fixed, stained for lipid droplets, labeled for perilipin, and imaged with a 10X objective (8 images/well were obtained, corresponding to approximately 2000 cells/well). A, The effect of rosi on the percentage of cells that expressed lipid droplets. B, The average number of lipid droplets per cell (lipid droplet count). C, The average lipid droplet diameter. D, The average pixel intensity of the lipid image for the lipid droplet mask. E, The average area of the protein mask (which corresponds to the perilipin mask in this experiment). Each bar is the mean \pm SD for $n = 6$ wells. Z' values were calculated between the sample groups corresponding to 0 vs. $1 \mu\text{M}$ (10^{-6}M) rosi. Asterisks (*, **, or ***) represent

$p < 0.05$, $p < 0.01$, or $p < 0.001$, respectively, vs. the controls (ANOVA followed by Dunnett's test),

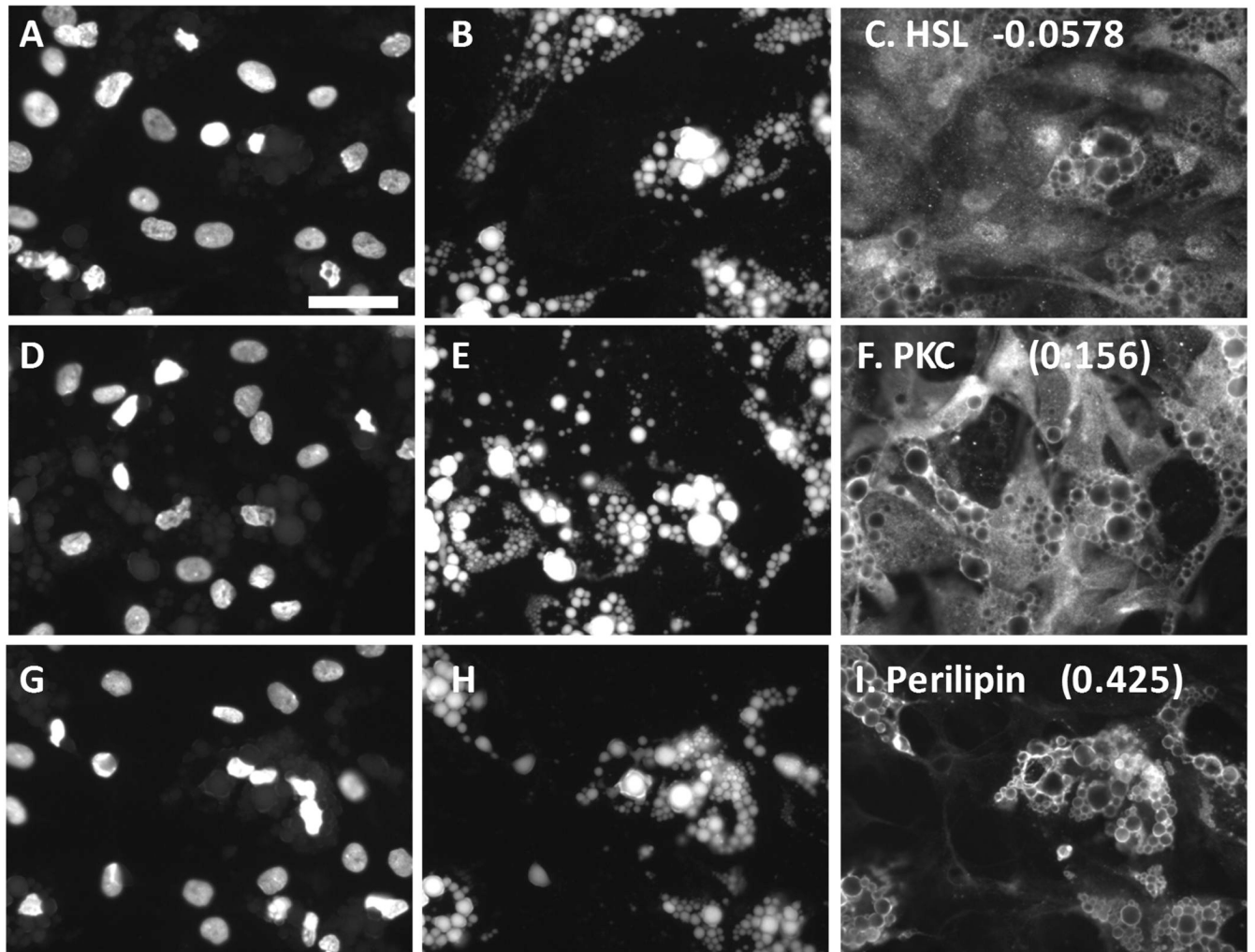


Figure 5. Quantification of protein - lipid droplet colocalization in human adipocytes

Human preadipocytes, plated in a 96-well dish, were exposed to 1000 nM of a proprietary PPAR γ agonist for 19 days, then fixed and stained for nuclei, lipid droplets, and certain proteins that vary in their association with lipid droplets. A, B, and C represent the same field of view imaged for nuclei, lipid, and hormone sensitive lipase (HSL), respectively. D, E, and F represent cells visualized for nuclei, lipid, and PKC. G, H, and I represent cells visualized for nuclei, lipid, and perilipin. $P_r Li Pi Wm$ averaged across all cells in the well are shown in C, F, and I (73 to 252 cells analyzed per well). Scale bar = 50 μm applies to all images (40X).

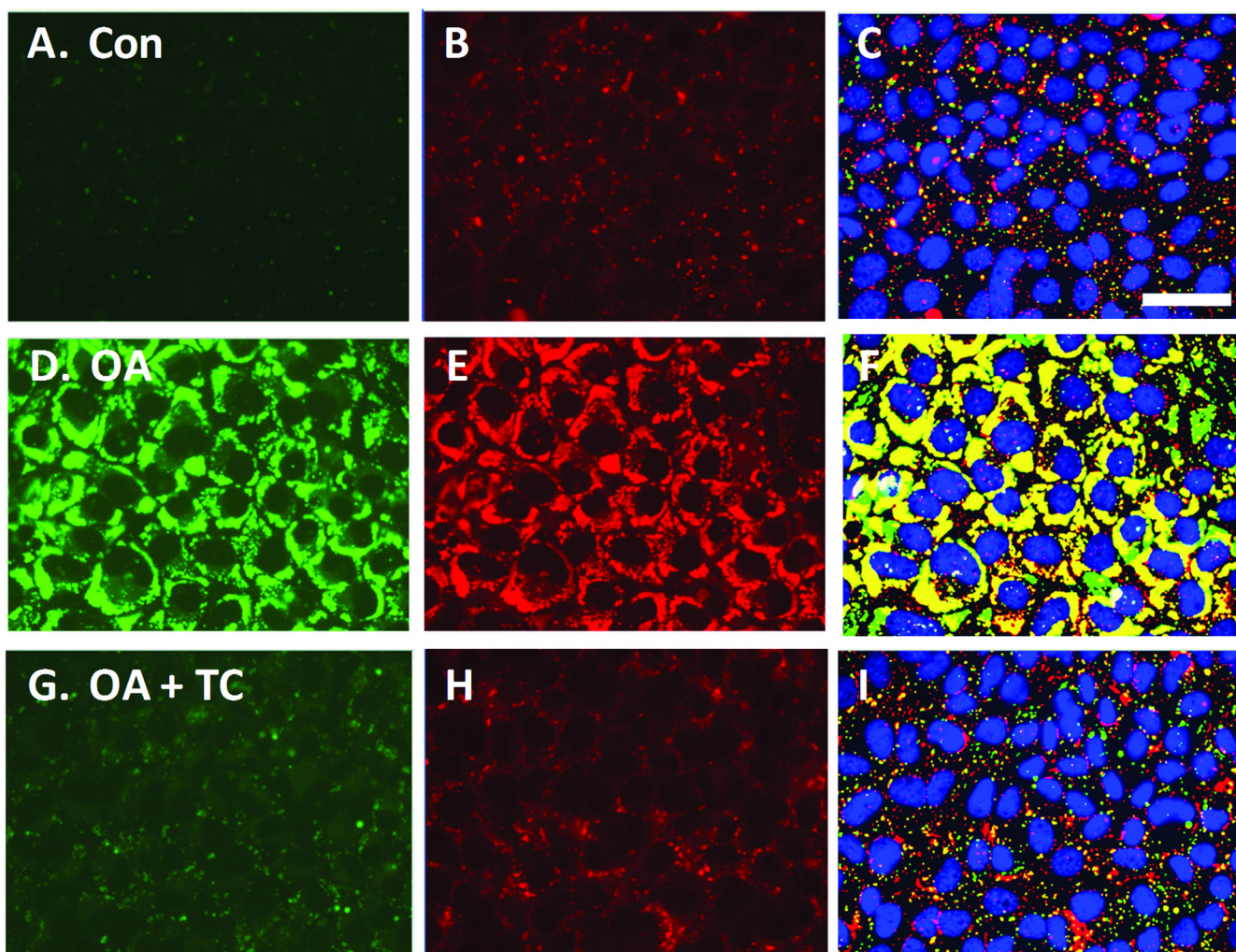


Figure 6. Effects of oleic acid (OA) and triacsin C (TC) on lipid droplet and ADFP expression in AML12 cells

Cells were cultured in a 96-well plate, then incubated with control media, 200 μ M OA or with OA plus 5.4 μ M TC, overnight. Cells were fixed, stained for lipid droplets, labeled for ADFP, then imaged (40X) and analyzed in an automated fashion. A, Control cells are shown, visualized for lipid droplets (green). B, The same field of view as A, visualized for ADFP (red). C, The Lipid droplet (green) and Protein masks (red) calculated by CyteSeer® for A and B are shown along with the nuclei (blue). Images D, E, and F, are from a field of view representing cells exposed to OA. G, H, and I are for cells exposed to OA plus 5.4 μ M TC. Images A, D, and G were optimized for brightness and contrast in an identical manner, so that faint lipid droplets within A and G could be more easily seen; images B, E, and H were also optimized identically, to increase visualization of ADFP in B and H. In the original images for D and E, pixel intensities were not saturated. Scale bar in A is 50 μ m, and applies to all panels.

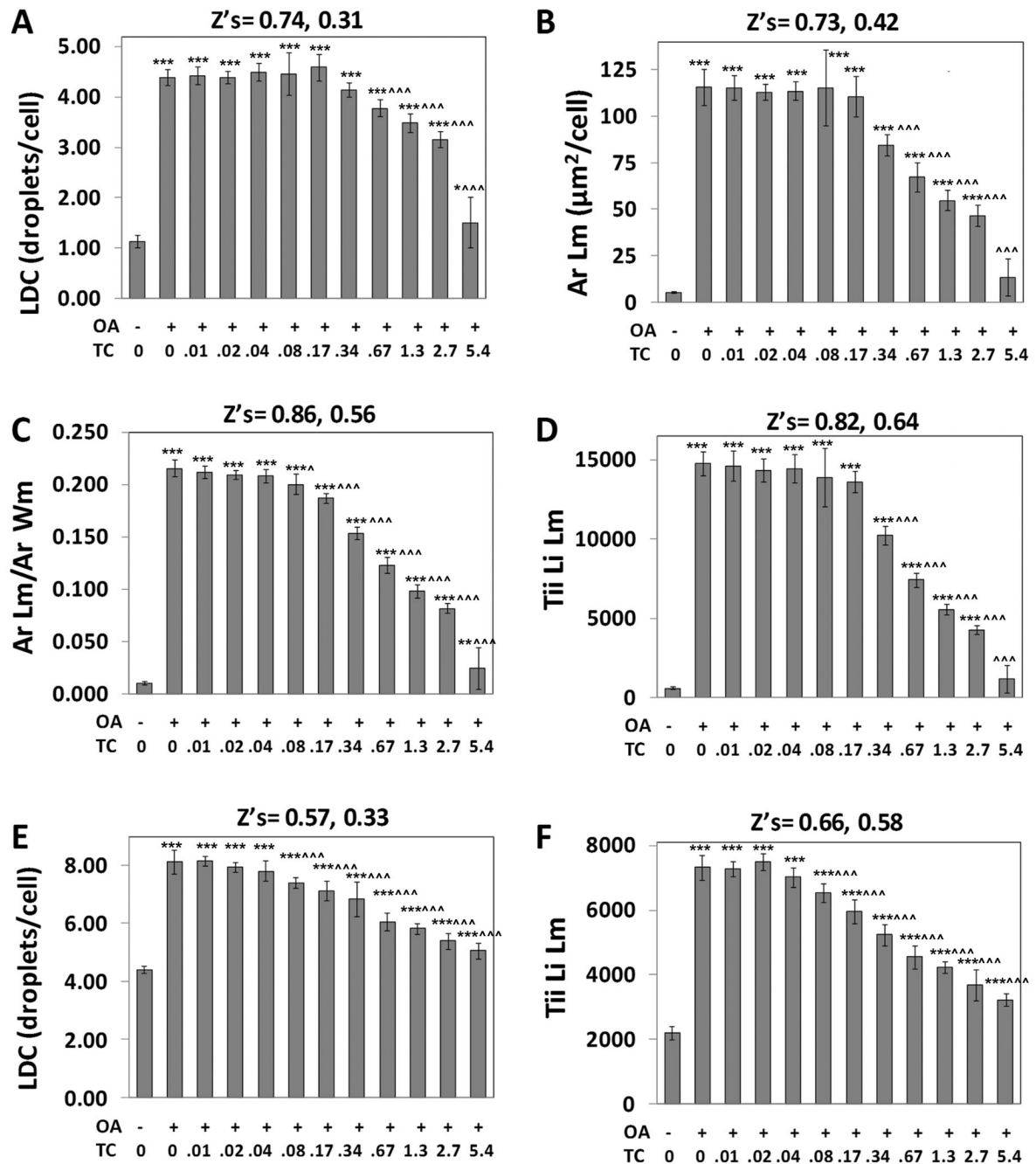


Figure 7. Quantification of oleic acid-induced lipid droplets in AML12 (A–D), and Huh-7 cells (E and F)

Cells were treated overnight with 200 μM oleic acid (OA) and triacsin C (TC, μM), as indicated. A, Lipid droplet count/cell (LDC) for AML12 cells. B, Average area of the Lipid droplet mask. C, Average area of the Lipid droplet mask normalized to the average area of the Whole cell mask. D, Total integrated intensity of the lipid image over the lipid droplet mask. E, Lipid droplet count (LDC) for Huh-7 cells. F, Total integrated intensity of the lipid image over the lipid droplet mask for Huh-7 cells. For A to E, cells were imaged with a 20X objective, and 4 images were analyzed per well (representing 632 to 1033 cells/well). For F, cells were imaged with a 10X objective, and 8 images were collected and analyzed per well (7340 to 9594 cells)

per well). For all panels, each bar represents the mean \pm SD for $n=8$ wells. The first Z' is for the effect of OA (calculated between 1st and 2nd columns); the second Z' is for the effect of 5.4 μ M TC in the presence of OA (calculated between the 2nd and final columns). Asterisks (*, **, or ***) represent $p < 0.05$, $p < 0.01$, or $p < 0.001$, respectively, vs. the control wells (first column), ANOVA followed by Newman Keuls post hoc analysis. Carets (^, ^^, or ^^) represent $p < 0.05$, $p < 0.01$, or $p < 0.001$, respectively, vs. wells treated with OA only (second column).

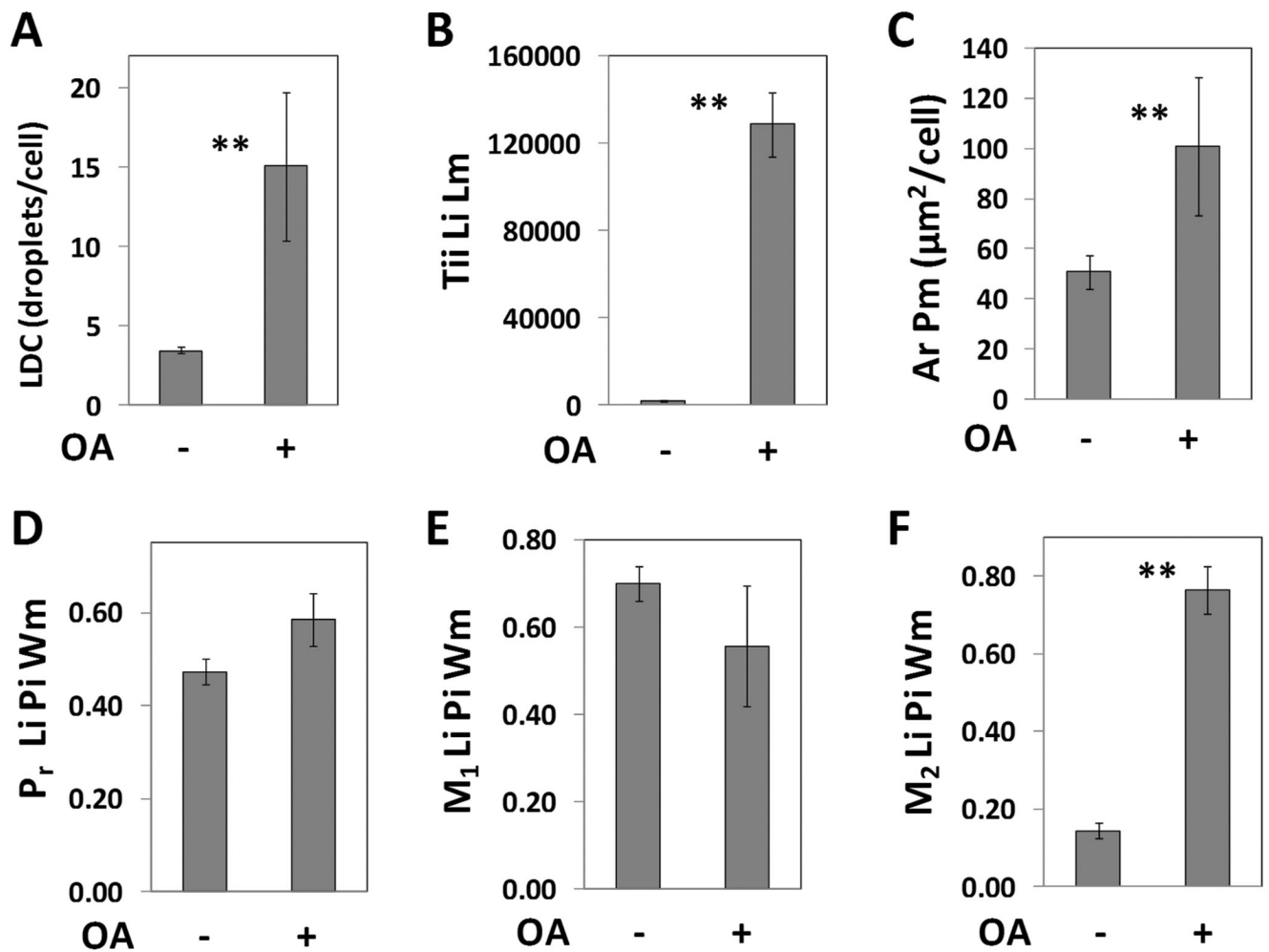


Figure 8. Analysis of lipid droplets and ADFP colocalization in AML12 cells

AML12 cells were cultured in the absence or presence of oleic acid (OA, 200 μM), processed as in Figure 7, and imaged with a 40X objective. A, Lipid droplet count (LDC). B, Total integrated intensity of the lipid image for the lipid mask. C, Area of the protein mask (ADFP in this experiment). D, Pearson's Correlation Coefficient for the lipid droplet and protein images calculated over the whole cell mask. E, and F are the Manders' M_1 and M_2 colocalization coefficients, also calculated for the Whole cell mask. Each bar represents the mean \pm SD for $n=7$ or 8 wells, with an average of 413 cells/well. ** $p < .01$ vs. control (ANOVA followed by Dunnett's test).

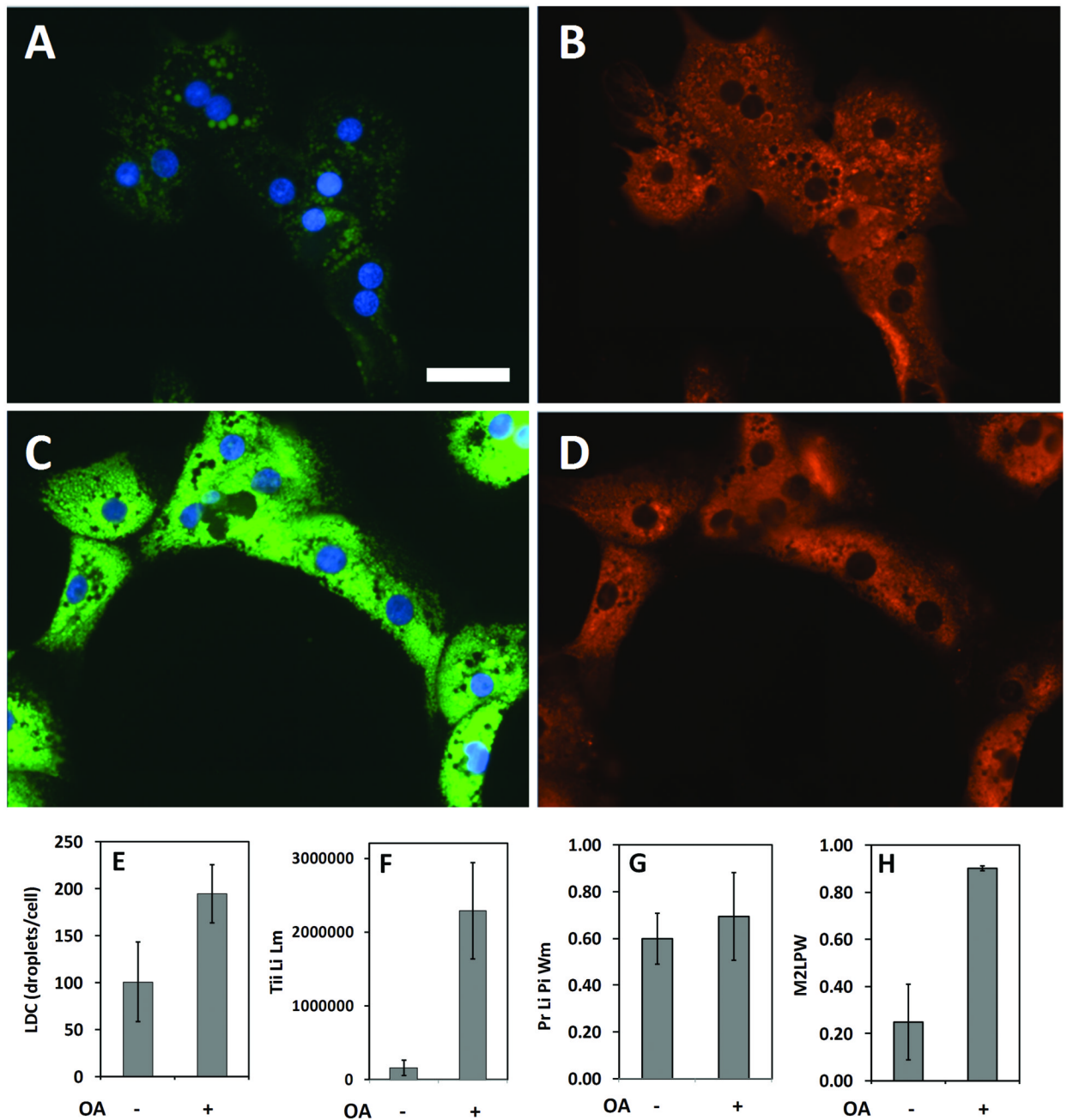


Figure 9. Quantification of lipid droplets and ADFP in primary rat hepatocytes

Hepatocytes, prepared from an adult rat, were cultured for 2 days in DMEM + 10% FBS in a 96-well dish. The cells were exposed to 200 μ M oleic acid (OA) overnight, then fixed and labeled for lipid droplets and ADFP. Control cells visualized (40X) for lipid droplets (green) plus nuclei (blue) are shown in A, and the corresponding ADFP (red) image is shown in B. OA-treated cells visualized in the same manner are shown in C and D. The scale bar is 50 μ m and applies to A–D. The number of lipid droplet count (LDC) and the total integrated intensity of the lipid image at the lipid mask are shown in E and F, respectively. G, and H depict the Pearson's Correlation and the Manders' M_2 coefficients calculated between the lipid droplet

and protein images over the whole cell mask, respectively. For E – H, each bar represents the mean \pm SD for n= 3 or 2 wells, respectively (5 to 112 cells/well were analyzed).

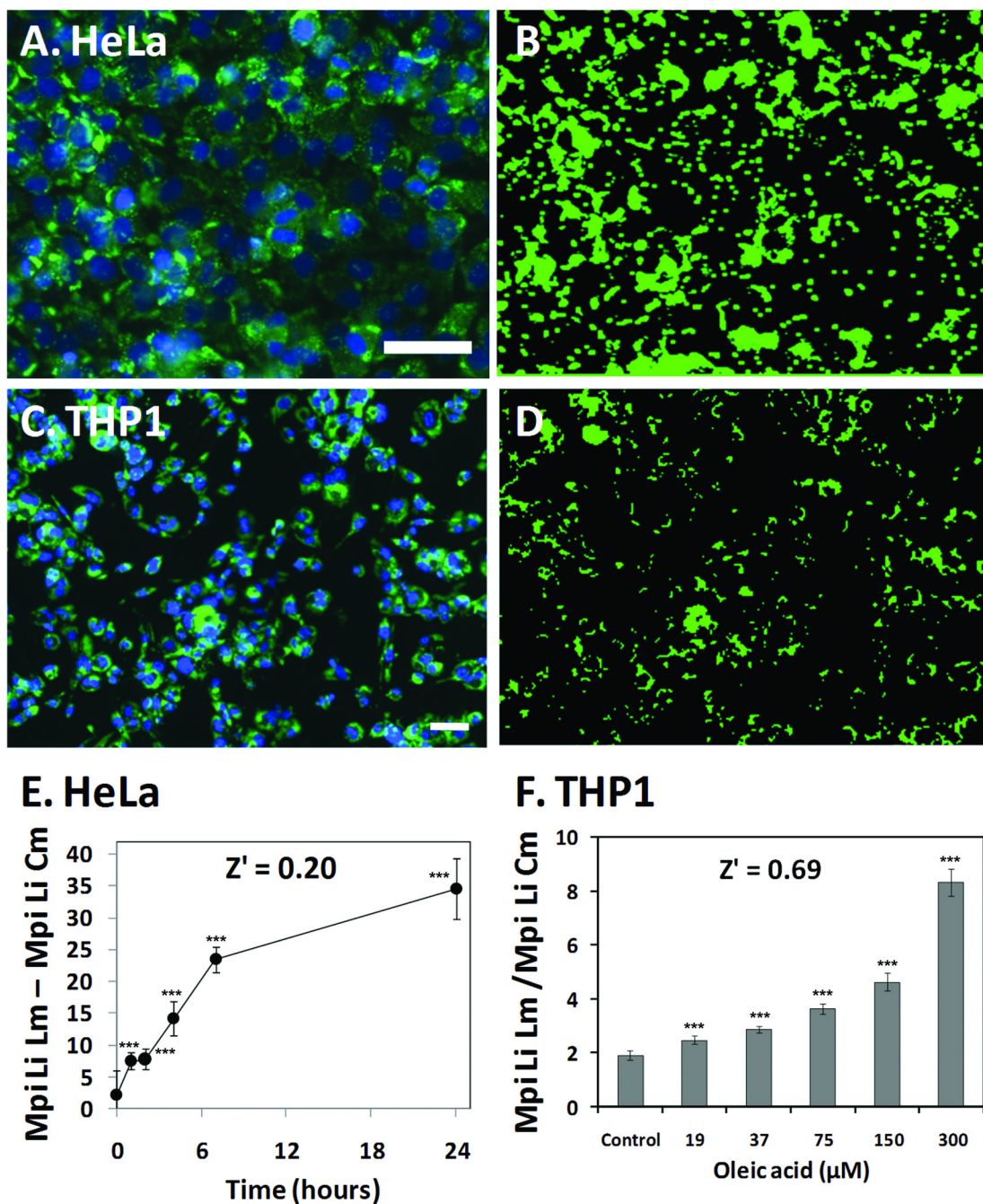


Figure 10. Quantification of lipid droplets in HeLa and THP-1 cells

A, HeLa cells are shown which have been stained for lipids (green) and nuclei (blue) following overnight exposure to 150 μM oleic acid. B) The Lipid droplet mask (green) derived from A is shown. C, THP-1 cells maintained in 100 nM PMA to induce differentiation to macrophages, stained for lipids and nuclei following overnight exposure to 150 μM oleic acid are shown. D, Lipid droplet mask (green) derived for the lipid droplets from C. E) Time course of lipid accumulation in HeLa is shown; the Y-axis is the difference in intensity between the median pixel intensities of the lipid mask vs. the cytoplasmic mask for the lipid image For THP1 cells, the dose-response for oleic acid induced accumulation of lipid is shown; The y axis is the ratio of the median pixel intensities of the lipid mask vs. the cytoplasmic mask for the lipid image.

For E and F, each bar represents the mean \pm SD for n=16 wells. Scale bars in A and D are 50 μ m. *** p < 0.001 vs. controls, ANOVA followed by Dunnett's test.

Table 1
Definitions and data parameters from CyteSeer®'s Lipid Droplet and Colocalization algorithms

Image channels and masks are abbreviated with two characters, where first letter refers to the cell structure being considered and the second letter (lower case) designates image (i) or mask (m) respectively; thus “Ni” is the nuclear image, whereas “Nm” is the nuclear mask. Area data (Ar) has units of $\mu\text{m}^2/\text{cell}$. Lipid droplet count (LDC) is per cell. Average and median pixel intensity (Api and Mpi) values ranged from 0 to 255, as the images in this study were 8-bit depth. Total integrated intensity is the sum of intensities for all pixels in the designated image and mask. For colocalization, L_i and L_{aver} refer to the individual-, and average-pixel intensities of the lipid image whereas $L_{i,coloc}$ is the pixel intensity within the lipid image for pixels that are also above threshold in the protein image. Similarly, P_i , and P_{aver} , refer to the individual-, and average- pixel intensities of the protein image and $P_{i,coloc}$, is pixel intensity within the protein image for pixels that are also above threshold in the lipid image. Pearson's Correlation (P_r) and the Manders' colocalization coefficients (M_1 and M_2) are dimensionless. P_r ranges from -1.0 (perfect exclusion) to 1.0 (perfect colocalization) with a value of 0 indicating a random distribution between the two labels; M_1 and M_2 range from 0 to 1.0.

<u>Image channels:</u>	<u>Masks:</u>	<u>Area and lipid droplets:</u>
Ni = Nuclear image (DAPI)	Nm = Nuclear	Ar Wm = Area Whole cell mask
Li = Lipid image	Wm = Whole cell	Ar Lm = Area Lipid mask
Pi = Protein image	Cm = Cytoplasm	Ar Pm = Area Protein mask
	Lm = Lipid	LDC = Lipid Droplet Count
	Pm = Protein	LDD = Lipid Droplet Diameter
<u>Pixel Intensity :</u>	<u>Colocalization:</u>	
Tii = Total integrated pixel intensity		
Api = Average pixel intensity		
Mpi = Median pixel intensity		
		$\text{Pearson's } P_r = \frac{\sum_i (L_i - L_{aver}) * (P_i - P_{aver})}{\sqrt{(\sum_i (L_i - L_{aver})^2 * \sum_i (P_i - P_{aver})^2)}}$
		$\text{Manders' } M_1 = \frac{\sum_i L_{i,coloc}}{\sqrt{\sum_i L_i}}, M_2 = \frac{\sum_i P_{i,coloc}}{\sum_i P_i}$
<u>Commonly used data parameters:</u>		
Tii Li Lm = Total integrated pixel intensity, Lipid image, Lipid mask		
Api Li Lm = Average integrated pixel intensity, Lipid image, Lipid mask		
Mpi Li Lm = Median pixel intensity, Lipid image, Lipid mask.		
P_r Li Pi Wm = Pearson's correlation, Lipid image, Protein image, Whole cell mask		
M_1 Li Pi Wm = Manders' M_1 , Lipid Image, Protein image, Whole cell mask		
M_2 Li Pi Wm = Manders' M_2 , Lipid Image, Protein image, Whole cell mask		

Table 2

Example data reports generated by CyteSeer®

Cell by cell readout: LDC, Area Lm, the Ratio of Area Lm/Area Wm, Tii Li Lm, Api Li Lm, and Mpi Li Lm are reported for an experiment with AML12 cells. Data is shown for the first 6 cells from well A1, out of a total of 914 cells that were imaged and analyzed for this well. Area Lm is in pixel units. **Well by well readout:** The number of cells (NOC) analyzed per well is shown, along with the mean values of the data parameters (averaged across all cells that were imaged in the well) for the first 6 wells in this experiment (out of a total of 96 wells). Additional population statistics can also be reported for each data parameter including medians and standard deviations. A1 is a control well, A2 received oleic acid which stimulates lipid droplet formation. Wells A3 – A6 received oleic acid plus increasing amounts of triacsin C, an inhibitor of lipid droplet formation (see Figure 7 for summary data).

Cell by cell readout:						
Well	Cell ID	LDC	Area Lm	Ratio (Lm/Wm)	Tii Li Lm	Mpi Li Lm
A1	1	2	22	0.0168	1093	49.7
A1	2	1	6	0.0036	207	34.5
A1	3	0	0	0.0000	0	0.0
A1	4	0	0	0.0000	0	0.0
A1	5	1	14	0.0086	489	34.9
A1	6	0	3	0.0012	70	23.3
.						46
.						35
.						0
.						0
.						35
.						22

Well by well readout (mean values):						
Well	NOC	LDC	Area Lm	Ratio (Lm/Wm)	Tii Li Lm	Mpi Li Lm
A1	914	1.12	12.5	0.010	530	32.0
A2	842	4.62	304.1	0.221	15005	48.4
A3	848	4.43	296.1	0.212	14322	47.4
A4	958	4.32	263.2	0.209	13520	50.4
A5	991	4.23	261.0	0.213	13277	50.0
A6	1005	3.96	237.6	0.193	11478	47.6
.						31.2
.						45.8
.						44.8
.						47.4
.						47.1
.						45.1

Table 3
P_r Li Pi Wm for human adipocytes as quantified by CyteSeer®

For Exp. 1, each data point represents a single well (73 to 252 cells/well). Since the P_r Li Pi Wm values for each protein were relatively constant across all agonist concentrations, the data points obtained for each well were averaged for comparison (final column).

Exp. 1		PPAR γ agonist (μ M)		
Protein	0.1	1	10	Mean \pm SD
HSL	0.0978	-0.0578	-0.0431	-0.00103 \pm 0.0859* (n=3)
PKC	0.156	0.156	0.167	0.160 \pm 0.00635* (n=3)
Perilipin	0.368	0.425	0.429	0.377 \pm 0.0483* (n=5)
	0.322	0.342		

Exp. 2		Rosi(1 μ M)
Perilipin		0.480 \pm 0.0691 (n=5)
HCS CellMask™		0.186 \pm 0.0437** (n=5)

* p < 0.05 vs. all other groups in Exp. 1 (ANOVA followed by Neuman Keuls post hoc analysis). For Exp. 2, cells were exposed to 1 μ M rosi for 17 days, then fixed and stained for lipids and labeled for either perilipin or HCS CellMask™; data points are the average \pm SD for n= 5 wells/condition (150 to 234 cells/well).

** p < .01, vs. perilipin, (Student's t-test).